OXFORD GENETICS

GENETICS, 2023, 225(1), iyad134
https://doi.org/10.1093/genetics/iyad134
Advance Access Publication Date: 19 July 2023
Investigation

Domains and residues of the *Saccharomyces cerevisiae* hnRNP protein Hrp1 important for transcriptional autoregulation and noncoding RNA termination

Emma C. Goguen, David A. Brow*

Department of Biomolecular Chemistry, University of Wisconsin School of Medicine and Public Health, Madison, WI 53706, USA

*Corresponding author: Department of Biomolecular Chemistry, University of Wisconsin School of Medicine and Public Health, 420 Henry Mall, Madison, WI 53706, USA. Email: dabrow@wisc.edu

Abstract

Proteins that bind the nascent transcript exiting RNA polymerase II can regulate transcription elongation. The essential *Saccharomyces cerevisiae* hnRNP protein Hrp1 is one such protein and participates in both cleavage and polyadenylation-coupled and Nrd1-Nab3-Sen1-dependent RNA polymerase II termination. Prior evidence that Hrp1 is a positive RNA polymerase II elongation factor suggests that its release from the elongation complex promotes termination. Here we report the effects of deletions and substitutions in Hrp1 on its autoregulation via an Nrd1-Nab3-Sen1-dependent transcription attenuator in the 5′-UTR of its mRNA and on the function of an Hrp1-dependent Nrd1-Nab3-Sen1 terminator in the *SNR82* snoRNA gene. Deletion of either of two central RNA recognition motifs or either of the flanking low-sequence complexity domains is lethal. Smaller, viable deletions in the amino-terminal low-sequence complexity domain cause readthrough of both the *HRP1* attenuator and *SNR82* terminator. Substitutions that cause readthrough localized mostly to the RNA recognition motifs, although not always to the RNA-binding face. We found that autoregulation of Hrp1 mRNA synthesis is surprisingly robust, overcoming the expected lethal effects of the start codon and frameshift mutations via overexpression of the mRNA up to 40-fold. Our results suggest a model in which binding of attenuator or terminator elements in the nascent transcript by RNA recognition motifs 1 and 2 disrupts interactions between RNA recognition motif 2 and the RNA polymerase II elongation complex, increasing its susceptibility to termination.

Keywords: RNA polymerase II, transcription termination, NNS termination, yeast, hnRNP proteins, transcription

Introduction

Accurate termination of RNA polymerase II (RNAP II) transcription is important for producing functional RNAs, recycling RNAP II, and preventing transcriptional interference between adjacent genes. The budding yeast *Saccharomyces cerevisiae* has two major termination pathways for RNAP II: cleavage and polyadenylation (CPA), which acts on most mRNAs, and Nrd1-Nab3-Sen1 (NNS) termination, which acts primarily on short, noncoding RNAs, including small nuclear RNAs (snRNAs), small nucleolar RNAs (snoRNAs), and cryptic unstable transcripts (Kuehner *et al.* 2011; Arndt and Reines 2015). The NNS pathway also regulates the synthesis of some mRNAs by attenuation of transcription via "leaky" NNS terminators in their 5′-untranslated regions. The NNS termination pathway is functionally analogous to the metazoan integrator-dependent termination pathway, although their factors and mechanisms are distinct (Wagner *et al.* 2023). The RNA-binding proteins Nrd1 and Nab3 and the RNA and DNA helicase Sen1 are the most well-characterized factors in the NNS pathway. Other proteins, including the RNA-binding protein Hrp1 and the phosphatase Ssu72, have been implicated in both the CPA and NNS pathways (Kessler *et al.* 1997; Dichtl *et al.* 2002; Ganem *et al.* 2003; He *et al.* 2003; Nedea *et al.* 2003; Steinmetz and Brow 2003; Kuehner and Brow 2008; Chen *et al.* 2017).

Termination of transcription requires slowing or pausing of elongation by RNAP II followed by its disengagement from the transcript and DNA template. Two general mechanisms have been proposed for the termination of RNAP II transcription (Rodríguez-Molina *et al.* 2023). The first, called the torpedo model, requires endonucleolytic cleavage of the nascent transcript to permit entry of a 5′-exonuclease that degrades the RNA emerging from RNAP II (Connelly and Manley 1988; Proudfoot 1989). Upon colliding with RNAP II the exonuclease induces termination by backtracking of RNAP II to release the transcript and/or altering RNAP II conformation. In a variant of the torpedo model a 5′-to-3′ translocase, analogous to the bacterial Rho termination factor, replaces the 5′-exonuclease, thus removing the requirement for transcript cleavage (Ray-Soni *et al.* 2016). Since there is no evidence of transcript cleavage in the NNS termination pathway, a torpedo mechanism would require a 5′-translocase. The helicase domain of Sen1 has 5′-to-3′ translocase activity on RNA and DNA and has previously been proposed to function by a mechanism analogous to Rho (Steinmetz and Brow 1996; Porrua and Libri 2013; Martin-Tumasz and Brow 2015; Han *et al.* 2017). The second mechanism, called the allosteric model, posits a change in transcription elongation complex (EC) conformation and/or composition upon encountering a terminator sequence

Received: May 04, 2023. **Accepted:** July 12, 2023

in the nascent transcript, which elicits termination (Logan *et al.* 1987). Current evidence suggests that torpedo and allosteric mechanisms may both contribute to termination by RNAP II (Luo *et al.* 2006; Rodríguez-Molina *et al.* 2023).

Hrp1, also called Nab4, is a candidate for directing allosteric termination of RNAP II. Hrp1 contains two adjacent RNA recognition motifs (RRMs) flanked by amino- and carboxyl-terminal low-sequence complexity domains (LCDs) (Fig. 1a). It was first identified as cleavage factor IB (Kessler *et al.* 1997), which is a component of the CPA termination complex and has been shown to be important for cleavage site selection in vitro (Minvielle-Sebastia *et al.* 1998). Later, Hrp1 was implicated in NNS termination by the discovery of negative autoregulation of synthesis of its mRNA via a leaky NNS terminator in the 5′-untranslated region (Steinmetz *et al.* 2006b; Kuehner and Brow 2008). This mechanism of autoregulation was first identified for Nrd1 (Steinmetz *et al.* 2001; Arigo *et al.* 2006). In addition to recognizing the NNS terminator in its own 5′-UTR, transcriptome analysis of an *hrp1* mutant strain revealed that Hrp1 promotes the NNS termination of several snoRNAs (Chen *et al.* 2017). A surprising additional finding from this study is that Hrp1 appears to act as a positive elongation factor for many mRNAs, as evidenced by a gradual decrease in RNA levels along the length of mRNAs in a metagene plot from an *hrp1* mutant strain. Given that Hrp1 crosslinks most efficiently to the 5′-end of mRNAs (Tuck and Tollervey 2013) and has been shown to ChIP to the gene body of several protein-coding genes (Licatalosi *et al.* 2002; Kim *et al.* 2006), we hypothesize that Hrp1 functions as an antitermination factor for RNAP II (Logan *et al.* 1987) and that its displacement from the EC in response to terminator elements in the nascent transcript promotes both CPA and NNS termination.

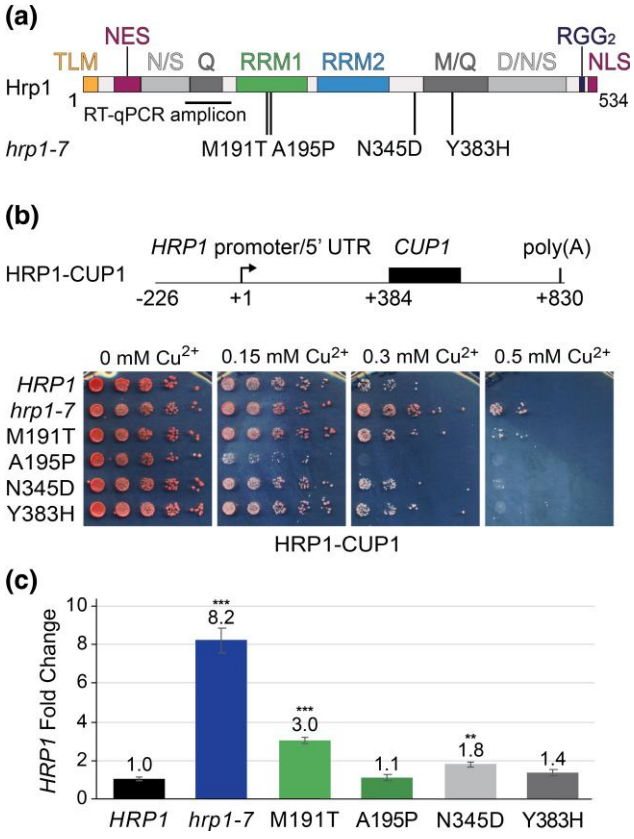

Fig. 1. Strong attenuator readthrough by *hrp1-7* requires more than one substitution. a) Domain structure of *S. cerevisiae* Hrp1. The N-terminal region contains an acidic sequence (TLM) that is highly conserved across fungi, a potential NES, and Asn/Ser-rich (N/S) and Gln-rich (Q) LCDs. The RRMs are shown in green and blue. The C-terminal region contains Met/Gln- (M/Q) and Asp/Asn/Ser-rich (D/N/S) LCDs, two Arg-Gly-Gly repeats (RGG_2), and a PY-type NLS. The *hrp1-7* substitutions are shown below. A horizontal black line marks the RT-qPCR amplicon. b) (top) Schematic diagram of the HRP1-CUP1 reporter. +1 indicates the most upstream transcription start site. (bottom) Serial dilutions of haploid strains containing the indicated alleles of *HRP1* and the HRP1-CUP1 reporter were spotted on medium containing the indicated concentration of copper sulfate. A biological replicate is shown in Supplementary Fig. 5a. c) RT-qPCR of total RNA from the indicated strains to produce the *HRP1* amplicon indicated in panel A. Values were normalized to a *CDC19* amplicon. Error bars represent the standard error of the mean (SEM) for 3 biological replicates. Significance between each mutant and wild-type was calculated by a 2-tailed Student's *t*-test indicated with *P*-value < 0.05 (*), <0.01 (**), or <0.001 (***).

To better understand the mechanism of Hrp1 function in NNS termination, we performed a mutational analysis of the protein to identify domains and residues required for this pathway. Because Hrp1 autoregulates synthesis of its mRNA via an NNS attenuator, decreased termination activity could be assessed both with reporter genes and by measuring levels of Hrp1 mRNA and protein. Using a reporter containing the terminator of the snoRNA gene *SNR82*, which is dependent on Hrp1 for efficient termination (Chen *et al.* 2017), we screened and selected for mutations in *HRP1* that cause readthrough. Most of these mutations fall into the tandem RRMs of Hrp1. Deletions, swaps, and duplications of the RRMs indicate that they have distinct and nonredundant essential functions. Terminator readthrough substitutions selected in a merodiploid strain, which must be dominant, were obtained primarily in the RNA-binding face of RRM1, while substitutions selected in a haploid strain, which must be viable, were obtained in both RRMs and, in RRM2, lie both within and outside the RNA-binding face. We found that Hrp1 autoregulation provides resilience to potentially lethal mutations, including substitutions in the start codon and a frameshift mutation, which result in strong upregulation of Hrp1 mRNA and near-normal expression of full-length (FL) Hrp1 protein. Our results are consistent with a model wherein Hrp1 acts as an antiterminator for the RNAP II EC that is anchored by RRM2 but releases upon binding to terminator elements in the nascent transcript.

Materials and methods

Plasmid construction

Supplementary Table 1 lists the plasmids used in this study. *HRP1* alleles were made in pRS313-HRP1(RI) containing −610 to +2,106 relative to the +1 ATG cloned into the BamHI and XhoI sites of pRS313 after PCR amplification with Hrp1 upstream and Hrp1 downstream with an EcoRI site added at position +1,649 downstream of the *HRP1* ORF by QuikChange with the primers pRS313-HRP1-EcoRI-F and pRS313-HRP1-EcoRI-R (Supplementary Table 3). pRS313-hrp1-7 was made by digesting pRS315-hrp1-7 (Kessler *et al.* 1997) with SacI and AvrII and ligation into SacI/AvrII digested pRS313-HRP1. Individual *hrp1-7* mutations A195P, N354D, and Y383H were made by QuikChange mutagenesis of pRS313-HRP1 (see Supplementary Table 3 for primers used). M191T was made by multiple fragment ligation followed by PCR as described in (An *et al.* 2010). A gene fragment (Azenta Life Sciences) containing *HRP1* sequence from +449 to +706 with the M191T substitution (T+572C) was digested with BstBI and AvrII, gel purified using the GeneJET Gel Extraction Kit (Thermo Scientific), and ligated with the following digested and gel purified fragments: SacI/EcoRI pRS313-HRP1, SacI/BstBI pRS313-hrp1-ΔRRM1, and AvrII/EcoRI pRS313-hrp1-ΔRRM1. The ligation products were PCR amplified with flanking primers and the correct-sized

product was gel purified, digested with SacI and EcoRI, and ligated into SacI/EcoRI pRS313-HRP1.

pGAC24-SNR82 was made by PCR amplification of +269 to +469 relative to the SNR82 start site with primers SNR82-downstream +269-F and SNR82-downstream +469-R containing XhoI sites and ligated into the XhoI site of the ACT1-CUP1 intron in pGAC24 (Lesser and Guthrie 1993).

The Hrp1 domain deletion constructs were made by inverse PCR of pRS313-HRP1 with primers that flanked the region to be deleted (Supplementary Table 3) followed by DpnI digestion, and self-ligation.

The pRS313-hrp1-RRM1dup, RRM2dup, and RRMswap strains were made by the same method as described for pRS313-hrp1-M191T. pRS313-hrp1-RRM1dup was made by ligating the following fragments: SacI/EcoRI pRS313-HRP1, SacI/AgeI pRS313-hrp1-ΔRRM2, NdeI/EcoRI pRS313-hrp1-ΔRRM2, and AgeI/NdeI RRM1dup gene fragment (containing RRM1 +478 to +702 in place of RRM2 +733 to +957). pRS313-hrp1-RRM2dup used the following fragments: SacI/EcoRI pRS313-HRP1, SacI/BstBI pRS313-hrp1-ΔRRM1, AvrII/EcoRI pRS313-hrp1-ΔRRM1, and BstBI/AvrII RRM2dup gene fragment (containing RRM2 +733 to +957 in place of RRM1 +478 to +702). pRS313-hrp1-RRMswap used the following fragments: SacI/EcoRI pRS313-HRP1, SacI/AvrII pRS313-hrp1-RRM2dup, NdeI/EcoRI pRS313-hrp1-RRM2dup, and AvrII/NdeI RRM1dup gene fragment.

pRS313-GFP-HRP1 was made by replacing the *HRP1* start codon in pRS313-HRP1 with the GFP (S65T) coding sequence using the NEB HiFi Assembly Master Mix according to the manufacturers guidelines. Primers GFP-HRP1-Fragment-F, GFP-HRP1-Fragment-R, GFP-HRP1-Vector-F, and GFP-HRP1-Vector-R were designed using SnapGene (Supplementary Table 3).

Yeast strains

See Supplementary Table 2 for yeast strains used in this study. Plasmids were transformed into *S. cerevisiae* by the lithium acetate procedure (Schiestl and Gietz 1989). ECG004 is derived from 46α (Lesser and Guthrie 1993). The *hrp1*::*KanMX4* disruption was made by PCR-amplification from the genomic DNA of BY4743 heterozygous diploid *HRP1*/*hrp1*::*KanMX4* (Dharmacon, clone Id 26273) with HRP1-ORF-F and HRP1-ORF-R primers (Supplementary Table 3 followed by digestion with NdeI to cut only *HRP1*, and gel extraction of *hrp1*::*KanMX4* using the GeneJet Gel extraction kit (Thermo Scientific). 46α containing pRS316-*HRP1* was transformed with the *hrp1*::*KanMX4* fragment and plated to yeast extract/peptone/dextrose (YEPD) media containing 0.5 mg/mL G418 disulfate (Alfa Aesar). Disruption of the chromosomal *HRP1* allele was confirmed by PCR and sequencing. pRS316-HRP1 was replaced with pRS313-bourne *HRP1* alleles by standard plasmid shuffle techniques (Boeke *et al.* 1987).

The viability of mutant alleles was determined by plating merodiploid strains onto synthetic complete media containing 5-FOA in biological triplicate. Alleles were considered inviable if all 3 biological replicates failed to grow on 5-FOA plates. If one replicate grew, plasmids were rescued from the 5-FOA viable strain and sequenced. In all cases, wild-type *HRP1* was detected either from a retained URA3-marked shuffle plasmid containing wild-type *HRP1* or loss of the mutation from the pRS313-HRP1 plasmid.

Genetic selections

The *HRP1* ORF was randomly mutagenized by error-prone PCR with HRP1-ORF-F and HRP1-ORF-R primers and Taq polymerase (Thermo Scientific) using the *Taq* Buffer containing KCl provided by the manufacturer, followed by PCR clean-up using the GeneJet Gel extraction kit. pRS313-HRP1 was digested with SacI and EcoRI by sequential digest and the vector backbone was gel purified using the GeneJET Gel Extraction Kit. The PCR product and SacI/EcoRI digested pRS313-HRP1-vector were cotransformed into ECG004 containing pGAC24-SNR82 and plated to a synthetic complete medium lacking histidine and leucine. The pRS316-HRP1 shuffle plasmid was removed by replica plating onto synthetic complete media containing 5-FOA. Colonies were subsequently replica plated onto SC media lacking leucine (Sunrise Scientific) and containing 0.15 mM $CuSO_4$. Plasmids were rescued from copper-resistant yeast colonies using the GeneJET Plasmid Miniprep Kit (Thermo Scientific) following cell lysis by vortexing with glass beads (425–600 μm diameter acid washed, Sigma-Aldrich) in kit Lysis Buffer for 2 minutes and a 5-minute incubation at 4°C. The plasmid mixture was then digested with NarI to cut only pGAC24-SNR82 and not mutagenized pRS313-*hrp1*, transformed into DH5α competent cells by standard heat shock transformation, and pRS313-*hrp1* plasmids were purified using the GeneJET Plasmid Miniprep Kit. The entire *HRP1* ORF of the pRS313-*hrp1* plasmids from the copper-resistant strains was sequenced to identify the mutations present.

The dominant selection was conducted as described above except the mutagenized *HRP1* PCR product and SacI/EcoRI digested pRS313-HRP1-vector were cotransformed into 46α containing pGAC24-SNR82. These transformants were then replica plated onto synthetic complete media lacking leucine and containing 0.15 mM $CuSO_4$. The pRS313-*hrp1* plasmids were rescued from copper-resistant strains as described above and were retransformed into naïve 46α strains containing pGAC24-SNR82. Eight-fold serial dilutions were conducted with 2 biological replicates on media lacking leucine and containing increasing concentrations of $CuSO_4$. The pRS313-*hrp1* plasmids were sequenced from strains where at least 1 biological replicate was copper resistant.

Protein analysis

For Hrp1 immunoblots, 10 OD units of yeast cells in log phase growth (OD_{600} of 0.5–1.0) at 30°C in YEPD or synthetic complete media lacking histidine were pelleted by centrifugation and lysed by vortexing with glass beads (425–600 μM diameter; Sigma-Aldrich) in 100 uL phosphate-buffered saline (PBS) (137 mM NaCl, 2.7 mM KCl, 10 mM Na_2HPO_4, 1.8 mM KH_2PO_4, pH 7.4) with Protease Inhibitor Cocktail V (Calbiochem). Then 100 uL 2x SDS-PAGE loading buffer (100 mM Tris–Cl, pH 6.8, 4% (w/v) SDS, 0.2% (w/v) bromophenol blue, 20% (v/v) glycerol, 200 mM 2-mercaptoethanol) was added, and the mixture was heated at 100°C for 5 minutes. Samples were electrophoresed using 4–15% Mini-PROTEAN TGX Precast Gels (Bio-Rad) at 100 V for 90 minutes and electroblotted onto PVDF membranes (Millipore) at 100 V, 4°C for 1 hour in 20% (v/v) methanol in Towbin buffer (25 mM Tris base, 192 mM glycine, pH 8.3). Blots were blocked with 5% dried milk in PBS buffer with 0.1% Triton X-100 at 23°C for 1 hour, incubated with affinity-purified Hrp1 antibody (1:5,000 dilution, Henry *et al.* 2003) for 1 hour at 23°C, and then with HRP-conjugated goat antirabbit IgG (Pierce Scientific) (1:20,000 dilution) for 1 hour. Blots were developed with Immobilon Western Chemiluminescent HRP substrate (Milipore Sigma) and were imaged using the Azure c600 imaging system. Band intensity was quantified using ImageJ (National Institutes of Health) and normalized to the total protein loaded. Total protein was measured by loading equal volumes of cell lysate onto 4–15% Mini-PROTEAN TGX Precast Gels (Bio-Rad), stained with Coomassie (45% (v/v) methanol, 10% (v/v) acetic acid, 3 g/L Coomassie brilliant blue R-250) for 1 hour, and destained in 50%

(v/v) methanol and 10% (v/v) acetic acid. The gel was imaged using the Azure c600 imaging system and the net absorbance of each lane with background subtracted was measured using ImageJ.

RNA analysis

Yeast cells were grown in YEPD at 30°C to an OD_{600} of 0.6–1.0 and pelleted by centrifugation. Total cellular RNA was prepared using the GeneJET RNA Purification Kit (Thermo Scientific) following cell lysis by vortexing with glass beads (200–325 um diameter, Sigma-Aldrich) in kit Lysis Buffer supplemented with DTT as directed by the manufacturer. Total RNA was treated with RNase-free DNase I (NEB) followed by purification with the GeneJET RNA Purification Kit according to the RNA clean-up protocol. RT-qPCR was conducted using the qScript One-Step SYBR Green qRT-PCR Kit (Quantabio) with 5 ng RNA in a 10 uL reaction volume (see Supplementary Table 3 for primers used). RNA concentration was measured on a Nanodrop One spectrophotometer (Thermo Scientific). RT-qPCRs were performed in technical triplicate using a Bio-Rad CFX384 Real-Time PCR detection system following the one-step qScript cycling protocol with the annealing/amplification temperature of 60°C. Data were analyzed using Bio-Rad's CFX Maestro program following the standard ΔΔCq method. To validate that each primer set amplified the correct gene, RT-PCR products were run on a 2% agarose gel, gel extracted, and sequenced (see Supplementary Table 3 for primers used). A No reverse transcriptase (No RT) control reaction was conducted with each primer set for each RNA sample. Each experiment containing 3 biological replicates and 3 technical replicates was conducted twice. Normalized fold change values between each mutant and wild-type were calculated for each experiment. The normalized values were then averaged together to calculate statistical significance. Significance was calculated by a 2-tailed unpaired Student's *t*-test.

Oligonucleotides

See Supplementary Table 3.

Results

The *HRP1* attenuator readthrough phenotype of *hrp1-7* is due to multiple substitutions

The primary structure of Hrp1 (Fig. 1a and Supplementary Fig. 1) is similar to that of human hnRNPD and DL, also called AUF1 and AUF1-like, respectively. The RRMs of the 3 proteins are most similar in sequence and share similarity with the tandem RRMs of the human Musashi-like proteins, Msi1 and Msi2, and DAZAP1 (Supplementary Fig. 2). Furthermore, the Hrp1 RRMs are highly similar to each other (38% identical and 55% similar; Supplementary Fig. 3b) and have previously been shown to bind the yeast polyadenylation efficiency element (UAUAUA) that is important for positioning the CPA machinery (Kessler *et al.* 1997; Chen and Hyman 1998).

Previous genetic studies of Hrp1 have primarily used a small number of heat-sensitive alleles (Kessler *et al.* 1997; Minvielle-Sebastia *et al.* 1998). We reported a transcriptome analysis using one of these alleles, *hrp1-7*, and found that it causes readthrough of some snoRNA terminators in addition to its own attenuator (Chen *et al.* 2017). The allele used in this study was previously thought to be *hrp1*-5 but subsequent sequencing identified 4 missense mutations: M191T and A195P in RRM1, and N345D and Y383H in a Met/Gln-rich low complexity region C-terminal to RRM2 (Fig. 1a and Supplementary Fig. 1; Kuehner and Brow 2019), which most closely matches the allele reported as *hrp1-7* (Kessler *et al.* 1997). When mapped on an NMR structure of the Hrp1 RRMs bound to $(UA)_4$ (Pérez-Cañadillas 2006), M191T is on the RNA binding face of RRM1, suggesting it disrupts RNA recognition, while A195P is in a loop and does not appear to make any RNA contacts (Supplementary Fig. 3a). To determine the contribution of each of the 4 substitutions to the heat-sensitive and readthrough phenotypes of this allele, we made each individual substitution and shuffled them into an *hrp1* disruption strain. We found that none is heat-sensitive on its own (Supplementary Fig. 4), indicating that a combination of at least two of the substitutions is required for this phenotype.

To determine which of these substitutions cause readthrough of NNS terminators, we used a reporter that contains the *HRP1* promoter and 5′ UTR fused to the *CUP1* protein-coding region and 3′ UTR, which confers copper resistance proportional to its expression level (Kuehner and Brow 2008). We transformed this reporter plasmid into an *hrp1* disruption strain containing *hrp1-7* or the individual mutations on low copy plasmids and spotted serial dilutions on plates containing increasing concentrations of copper sulfate (Fig. 1b and Supplementary Fig. 5a). Consistent with previous results (Kuehner and Brow 2008), the *hrp1-7* allele conferred copper resistance up to 0.5 mM indicating that it causes strong readthrough of the *HRP1* attenuator. Of the individual substitutions, *hrp1-M191T* confers the most copper resistance and appears to be largely responsible for the readthrough phenotype of the quadruple mutant. Both *hrp1-N345D* and *hrp1-Y383H* cause weak readthrough. Interestingly, *hrp1-A195P* caused a decrease in copper resistance compared to wild-type *HRP1* in both biological replicates tested, suggesting that this substitution decreases the expression of the reporter, possibly by decreasing the positive elongation function of Hrp1.

To quantify changes in *HRP1* expression caused by the substitutions, we used RT-qPCR to measure *HRP1* mRNA levels from the plasmid-borne wild-type or mutant alleles (Fig. 1c). *hrp1-7* strains have 8-fold more *HRP1* mRNA than strains with wild-type *HRP1* (Fig. 1c), similar to the 4- to 5-fold increase in Hrp1 mRNA observed previously by Northern blot (Kuehner and Brow 2008). Consistent with the HRP1-CUP1 reporter results, *hrp1-M191T* produced the largest increase in *HRP1* mRNA levels of any single substitution, but substantially less than *hrp1-7*. *hrp1-N345D* was the only other single substitution that produced a significant, albeit small, increase in *HRP1* mRNA. Interestingly, this substitution is adjacent to an RGG motif that is conserved in human hnRNPD and DL (Supplementary Fig. 2). The A195P substitution did not cause a significant decrease in *HRP1* mRNA levels, possibly because the elongation defect inferred from the HRP1-CUP1 reporter assay is offset by increased readthrough of the *HRP1* attenuator due to lowered Hrp1 levels. Our results suggest that RRM1 RNA binding is important for Hrp1 termination activity and that at least the N345D substitution in the carboxyl-terminal low complexity domain enhances the readthrough phenotype.

The *SNR82* terminator is stronger than the *HRP1* attenuator but responds similarly to *hrp1-7* substitutions

Our previous transcriptome analysis showed that the *hrp1-7* allele causes readthrough of several snoRNA gene terminators (Chen *et al.* 2017), including the *SNR82* gene (Fig. 2a). To assess the effects of individual *hrp1-7* substitutions, we used RT-qPCR with primer pairs that amplify a region within the *SNR82* gene (5′ amplicon) and a region between *SNR82* and *USE1* (3′ amplicon). The 3′ amplicon is expected to detect the primary *SNR82* transcript that has not yet been 3′-trimmed by the exosome as well as the

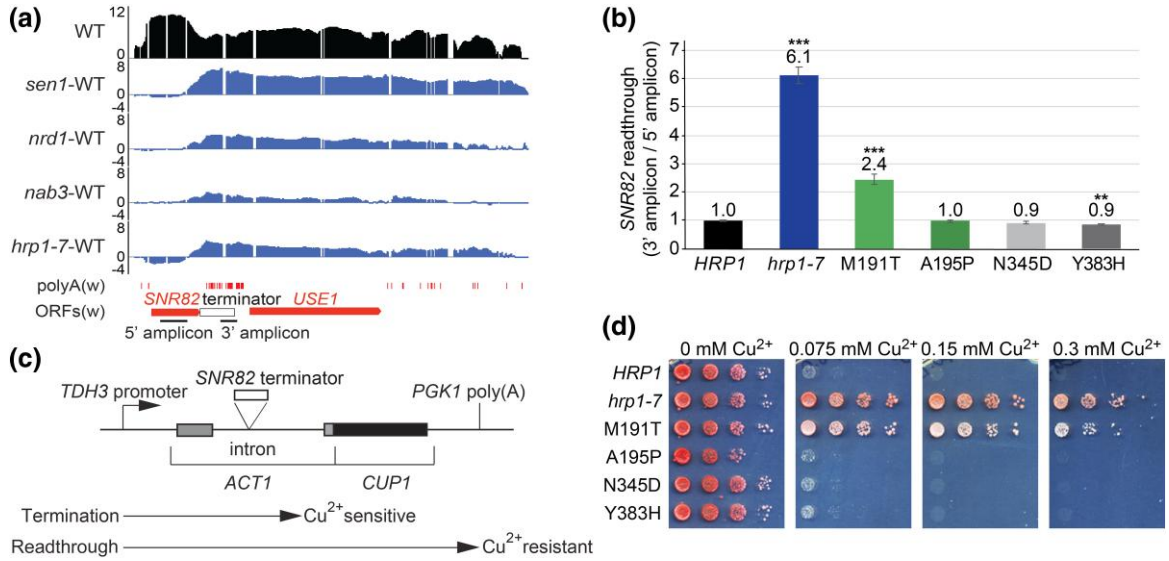

Fig. 2. Confirmation of *SNR82* terminator readthrough in the presence of *hrp1-7*. a) Transcriptome data of NNS mutants including *hrp1-7* from (Chen *et al.* 2017). The y-axis is a log2 scale with wild-type RNA levels in black and fold change in transcript levels for the mutants in blue. Annotated genes and mapped poly(A) 3′ ends (Ozsolak *et al.* 2010) in the top (w) strand are shown in red. The *SNR82* terminator region is indicated by a white box and RT-qPCR amplicons by black lines. b) *SNR82* terminator readthrough in strains containing the indicated *HRP1* alleles calculated as the ratio of 3′ to 5′ RT-qPCR amplicons, normalized to wild-type *HRP1*. Error bars represent the SEM for 3 biological replicates. Significance between each mutant and wild-type was calculated by a 2-tailed Student's *t*-test indicated with *P*-value < 0.05 (*), <0.01 (**), or <0.001 (***). c) Schematic of the *ACT1*-CUP1 reporter construct containing the *SNR82* terminator region (white box in panel a). d) Serial dilutions of haploid strains containing the indicated alleles of *HRP1* and the *SNR82 ACT1*-CUP1 reporter on separate plasmids were spotted on medium containing the indicated concentration of copper sulfate. Biological replicate shown in Supplementary Fig. 5b.

SNR82-USE1 readthrough product. Readthrough of the *SNR82* terminator was measured as the ratio of 3′ amplicon/5′ amplicon for the mutant divided by the same value for wild-type *HRP1*. Consistent with the transcriptome data, *hrp1-7* has a 6-fold increase in readthrough compared to wild-type *HRP1* (Fig. 2b). *hrp1-M191T* was the only single substitution that exhibited significant readthrough and contributed a nearly identical fraction of the readthrough activity of *hrp1-7* as for the *HRP1* attenuator (39% vs 37%). Thus, for both NNS terminators one or more of the other substitutions in *hrp1-7* increases readthrough more than 2-fold. Unlike the *HRP1* attenuator, the N345D substitution has no measurable effect on the *SNR82* readthrough on its own.

Having confirmed that the *SNR82* terminator is Hrp1-dependent, we incorporated the terminator in a reporter construct for further studies. We cloned a 200 base pair DNA fragment immediately downstream of the mature RNA-coding region of the *SNR82* gene into the intron of the *ACT1*-CUP1 reporter (Lesser and Guthrie 1993) that we used previously to characterize other NNS terminators (Steinmetz and Brow 1996, 2003; Steinmetz *et al.* 2006a) (Fig. 2a and c, and Supplementary Fig. 6). Readthrough of the *SNR82* terminator in the *ACT1* intron leads to expression of *CUP1* and allows the cells to grow on media containing copper sulfate. We conducted serial dilutions with *hrp1-7* and the individual substitution strains on media containing increasing concentrations of copper sulfate and found that these results correlate well with RT-qPCR of the endogenous *SNR82* gene, indicating that the region we cloned into the reporter acts as a strong terminator and is Hrp1-dependent (Fig. 2d and Supplementary Fig. 5b). The wild-type *HRP1* strain containing the *SNR82* reporter was unable to grow on even the lowest copper concentration tested (0.075 mM), indicating that the *SNR82* terminator is much stronger than the *HRP1* attenuator (Fig. 1b and Supplementary Fig. 5). In contrast, in the presence of *hrp1-7* the reporter conferred resistance to the highest copper concentration tested (0.3 mM). *hrp1-M191T* was the only single substitution that conferred copper resistance, which, as expected, was not as strong as for *hrp1-7*.

The amino- and carboxyl-terminal low complexity domains of Hrp1 are essential

Little is known about the contribution of domains outside the RRMs to Hrp1 function. As a first step in characterizing the functional domains of Hrp1 we used amino acid composition, sequence conservation, and secondary structure prediction to delineate regions of interest (Fig. 3a and Supplementary Fig. 1). We then deleted each region individually and assessed the recessive viability of each allele. We found that deletion of the entire region amino-terminal to the RRMs (ΔN-term) is recessive lethal (Supplementary Fig. 7a). Based on the AlphaFold prediction this region is largely unstructured (Jumper *et al.* 2021; Varadi *et al.* 2022), but we divided it into 4 regions based on amino acid composition and conservation among the *Saccharomycetaceae* yeasts (Supplementary Figs. 1 and 8). The first 15 amino acids are highly acidic and well-conserved across fungi (Supplementary Fig. 9), and resemble the TFIIS N-terminal domain interacting motif (TIM) found in many RNAP II elongation factors (Cermakova *et al.* 2021). We, therefore, named it the TIM-like motif (TLM). We found that the TLM is dispensable for viability, though it causes mild heat sensitivity at 37°C (Supplementary Figs. 7 and 10). Likewise, individual deletion of a predicted α-helical region we called nuclear export signal (NES) because it contains a putative nuclear export sequence (Henry *et al.* 2003) as well as the asparagine-serine (N/S)- and glutamine (Q)-rich amino terminal low complexity domains (LCDs) were viable (Supplementary Fig. 7b and c). A previous study showed that deletion of a region that spanned the N/S and Q LCDs caused cytoplasmic aggregates of Hrp1 to form when overexpressed (Newby *et al.* 2017). Thus, the amino-terminal LCDs increase the solubility of Hrp1. In contrast,

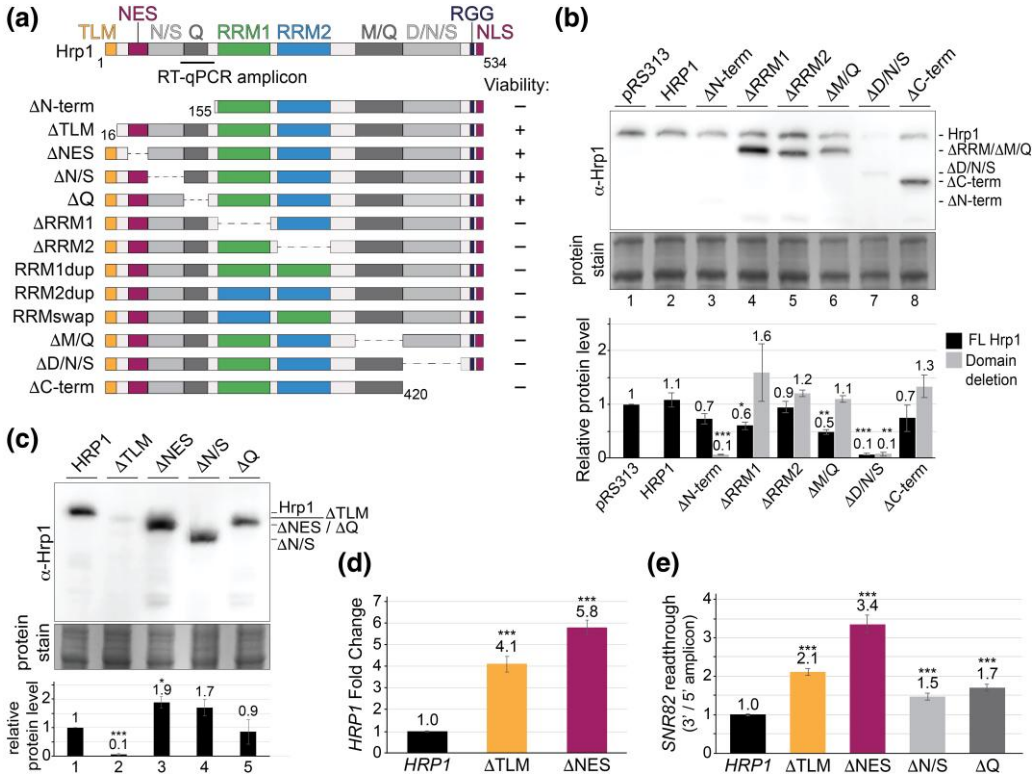

Fig. 3. Effects of Hrp1 domain deletions on cell viability, protein level, and readthrough. a) Schematic of Hrp1 primary structure and alleles tested in this study. Abbreviations are as in Fig. 1a. Viability in a haploid strain after 5 days of growth at 30° on medium containing 5-FOA is indicated at right (see Supplementary Fig. 7). Amplicon for RT-qPCR shown with a black line. b) Anti-Hrp1 Western blot of cell extracts from merodiploid strains containing chromosomal wild-type *HRP1* and the indicated *HRP1* alleles on a low copy number plasmid. A duplicate Coomassie blue stained gel, part of which is shown below, was used to normalize for total protein loaded. The average protein levels normalized to endogenous Hrp1 (lane 1) from 2 biological replicates (see Supplementary Fig. 11a) are shown in the graph below the gel with the FL Hrp1 shown in black and the domain deletions shown in gray for each strain. Error bars represent the SEM and significance between each mutant and wild-type was calculated by a 2-tailed Student's *t*-test indicated with *P*-value < 0.05 (*), <0.01 (**), or <0.001 (***). c) Anti-Hrp1 Western blot of cell extracts as in Panel B except from haploid strains containing the indicated viable *HRP1* alleles. d, e) RT-qPCR of total RNA from the indicated haploid strains to produce d) the *HRP1* amplicon indicated in panel a normalized to a *CDC19* amplicon or e) the *SNR82* 5′ and 3′ amplicons indicated in Fig. 2a. Error bars represent the SEM for 3 biological replicates for ΔTLM and ΔNES and 2 biological replicates for ΔN/S and ΔQ. Significance between each mutant and wild-type was determined as in panel b.

deletion of the carboxyl-terminal LCDs prevents aggregation of Hrp1 when overexpressed (Newby *et al.* 2017), indicating that this region promotes aggregation.

We divided the carboxyl-terminal low complexity region into two segments, a methionine and glutamine (M/Q)-rich region and an aspartate, asparagine, and serine (D/N/S)-rich region (Fig. 3a and Supplementary Fig. 1). The Reines lab showed previously that deletion of a region of Hrp1 corresponding closely to the M/Q LCD is recessive lethal (Loya *et al.* 2017) and we confirmed their finding (Supplementary Fig. 7c). We also found that the D/N/S LCD is required for viability (Supplementary Fig. 7g). Not surprisingly, deletion of the entire region carboxyl-terminal to the M/Q LCD (ΔC-term), which includes the Arg-Gly-Gly (RGG) repeats and essential nuclear localization signal (NLS) (Lange *et al.* 2008) is lethal (Supplementary Fig. 7h). Thus, both the amino- and carboxyl-terminal LCDs of Hrp1 are required for its essential function(s).

Hrp1 RRMs 1 and 2 have distinct essential functions

Given the high degree of similarity between RRM1 and RRM2 (Supplementary Fig. 3b), we tested if they function in a redundant manner. Deletion of either RRM alone was lethal (Fig. 3a and Supplementary Fig. 7d), indicating either that the 2 RRMs have distinct functions or that they have identical functions, but 2 copies must be present. To test the latter possibility, we replaced RRM2 with RRM1, creating a version of Hrp1 with 2 RRM1s (RRM1dup), and vice versa (Fig. 3a). Neither the RRM1dup nor RRM2dup version of Hrp1 is viable (Supplementary Fig. 7e and f), indicating the 2 RRMs have distinct molecular functions. To test if the functions are position-dependent, we constructed an "RRM swap" allele, in which RRM1 and RRM2 trade positions. Yeast containing only this allele of Hrp1 is also inviable (Supplementary Fig. 7f). We therefore conclude that RRM1 and RRM2 of Hrp1 mediate distinct, essential interactions that are position-dependent. These interactions could be intramolecular, intermolecular, or both.

Deletion of some domains of Hrp1 alter its level in cells

The inviability of Hrp1 lacking different domains could be due to decreased accumulation of mutant protein. Conversely, a mutant Hrp1 that has a dominant negative effect on attenuator function could be overexpressed. To assess the steady-state level of inviable deletion proteins, we conducted Western blots with anti-Hrp1 polyclonal antibody (Henry *et al.* 2003) on extracts from merodiploid strains containing chromosomal wild-type *HRP1* and each of the recessive lethal deletions on a low copy (centromere) plasmid (Fig. 3b and Supplementary Fig. 11a). When an additional copy of wild-type *HRP1* is introduced on a

plasmid, no significant increase in total Hrp1 protein is observed compared to the empty plasmid control (Fig. 3b, cf. lanes 1 and 2). This is as expected since autoregulation via Hrp1-dependent NNS attenuation should compensate for the increased gene dosage. The signal for ΔN-term Hrp1 (Fig. 3b, lane 3) is about 10% of wild-type, which could be due either to a low level of protein or to the absence of a major epitope for the polyclonal Hrp1 antibodies. In contrast, the individual RRM deletions and the M/Q LCD and C-term deletions results in at least as much mutant protein as wild-type Hrp1 (Fig. 3b, lanes 4-6 and 8). This finding implies that the inviability of these deletions is not due to loss of protein.

Unexpectedly, the D/N/S LCD deletion (Fig. 3b, lane 7) results in reduced amounts of both mutant and wild-type protein. It is possible that the absence of the D/N/S LCD results in a dominant gain-of-function that increases recognition of the *HRP1* attenuator on both the mutant and wild-type alleles by shifting the balance between elongation and termination (see Discussion). The dominant effect of the D/N/S allele appears to require Hrp1 nuclear localization as the C-term deletion that is lacking the NLS and the D/N/S LCD does not cause reduced Hrp1 protein level (Fig. 3b, lanes 7 and 8).

The steady-state levels of the recessive viable forms of Hrp1 were determined by shuffling plasmid-borne alleles into an *hrp1* disruption strain (Fig. 3c and Supplementary Fig. 11a). The ΔTLM strain appears to have much lower levels of Hrp1 protein but, as for ΔN-term Hrp1, this could be because either less protein accumulates or, more likely, this region contains an important epitope for the antibody. ΔNES was the only recessive viable deletion that caused a significant increase in Hrp1 expression compared to wild-type.

For the recessive viable deletions, a defect in function or stability may be masked by increased expression due to the readthrough of the *HRP1* attenuator. To determine if these alleles produce increased levels of Hrp1 mRNA, we conducted RT-qPCR with *HRP1* primers as described above. We did not test ΔN/S or ΔQ as the primers anneal within these deletions (Fig. 3a). We found that the ΔTLM and ΔNES alleles produce 4- to 6-fold more mRNA than wild-type *HRP1*, consistent with these deletions causing increased readthrough of the *HRP1* attenuator (Fig. 3d). Whether this effect is due to decreased protein function or disruption of the *HRP1* attenuator by the deletions, or both, is not clear. The *NRD1* attenuator is known to extend into the 5′ end of its coding region (Arigo *et al.* 2006) and this could be true for *HRP1* as well. Therefore, we also determined the effects of these deletions on readthrough of the endogenous *SNR82* terminator (Fig. 3e). ΔTLM and ΔNES caused 2- to 3-fold readthrough of the *SNR82* terminator, indicating that these regions of the protein are important for Hrp1 function at another terminator. Although the magnitude of their effects is less on a strong terminator than the *HRP1* attenuator, in both cases ΔNES causes more readthrough than ΔTLM. ΔN/S and ΔQ had a smaller, but significant effect on *SNR82* terminator readthrough (Fig. 3e). These results show that the amino-terminal region of Hrp1 encompassing the TLM and NES regions is important for its function at 2 NNS terminators.

Readthrough substitutions in the Hrp1 RRMs imply both shared and unique functions

Our deletion analysis showed that many Hrp1 domains are essential for viability and that the deletion of nonessential domains can cause a readthrough of two NNS terminators. We next sought to identify important residues for Hrp1 function at NNS terminators. We, therefore, conducted a genetic selection for viable mutations in *HRP1* that cause readthrough of the *SNR82* terminator. The entire *HRP1* ORF was randomly mutagenized by error prone PCR and the amplicon pool and a gapped *HRP1* plasmid lacking the ORF were cotransformed into a strain that has the genomic *HRP1* ORF replaced with an antibiotic resistance gene, wild-type *HRP1* on a *URA3*-marked plasmid, the *CUP1* locus deleted, and the ACT1-CUP1 reporter containing the *SNR82* terminator on a *LEU2*-marked plasmid. After the selection for repair of the gapped plasmid with the amplicon pool, loss of the wild-type copy of *HRP1* was selected by replica plating onto media containing 5-FOA, which required the transformed *HRP1* alleles to be viable. We then selected for readthrough of the *SNR82* terminator by replica plating onto -Leu medium that contained 0.15 mM $CuSO_4$. The *HRP1* plasmids were extracted from copper-resistant strains and the ORF was sequenced to identify any mutations present.

Based on our antiterminator model of the Hrp1 function, the selected mutations could disrupt terminator recognition and/or prevent the subsequent release of Hrp1 from the EC. We obtained 29 alleles from this selection. Two had no mutations in the *HRP1* 5′ UTR, ORF, or 3′ UTR and 1 (*hrp1-130*, Table 1) had no mutations in the *HRP1* ORF but contained 2 single-nucleotide substitutions in the 5′ UTR and a single-nucleotide deletion in the 3′ UTR. These 3 strains were not further studied. The remaining 26 alleles contained from 1 to 3 nonsynonymous substitutions or, in 2 cases, the same single-nucleotide deletion in the *HRP1* ORF (*hrp1*-125 and -127, Table 1). Most of the substitutions are in the RRM domains and most of the mutations in the amino- or carboxyl-terminal domains are in alleles that also contain a substitution in either of the RRMs. The exceptions are 2 strains with substitutions in the start codon and the 2 strains with the frameshift mutation in the C-terminal domain (see next section).

We mapped the 13 single amino acid substitutions in RRM1 or RRM2 onto an NMR structure of the Hrp1 RRMs with $(UA)_4$ RNA-bound (Pérez-Cañadillas 2006) (Fig. 4a and b). The substitutions in RRM1 are either in residues that appear to contact the RNA or are buried in the core of RRM1 and would likely destabilize the domain. Tryptophan168 stacks on an adenine nucleobase (Fig. 4b, i). We obtained the W168R mutation both in combination with the E21K substitution between the TLM and NES, and on its own (Table 1). Other substitutions in this residue, W168F and W168A, were previously shown to decrease the binding affinity of Hrp1 to UAUAUA RNA in vitro (Pérez-Cañadillas 2006). A recent study found that the W168F substitution reduces expression of *lacz* fused downstream of the *HRP1* attenuator about 2-fold, suggesting decreased readthrough of the attenuator (Amodeo *et al.* 2023). However, this effect could be due to decreased positive elongation activity on the bacterial gene rather than increased terminator recognition. The same study showed that the Hrp1-W168A substitution is recessive lethal.

Notably, we obtained in the selection the M191T substitution from the *hrp1-7* allele that causes readthrough of both the *HRP1* attenuator and *SNR82* terminator (Figs. 1 and 2). The sulfur atom of M191 forms an apparent n-π^* contact with a uracil base, as observed in another ribonucleoprotein (Nomura *et al.* 2018). M191 appears to be part of a "3-bridge cluster" (Gibbs *et al.* 2021) with F162 in beta-strand 1 and F202 and F204 in beta-strand 3, which also contact U5, A6, and U7 (Fig. 4b, ii). An F204L substitution was obtained in combination with another substitution (*hrp*-116), supporting the importance of this aromatic cluster.

The backbone carboxyl of R232 forms hydrogen bonds with the A6 base and the R232G substitution would likely alter the conformation of the carboxyl-terminal end of RRM1 and disrupt this interaction and a salt bridge with A233 (Fig. 4b, iii). R236 in the

Table 1. *HRP1* alleles selected in the absence of wild-type *HRP1* for readthrough of the *SNR82* terminator.

hrp1 allele	Amino acid substitution (nucleotide substitution)					
	5′ UTR:	N-term:	RRM1:	RRM2:	C-term:	3′UTR:
110		E21K (G61A)	W168R (T502C)			
111				V247A (T740C, T741G), C301R (T901C)		
112			G180G (T540C)	L274P (T821C)	P336L (C1097T)	
113			**W168R (T502A)**		R506R (T1518C)	
114				**K244N (A732C)**		
115			**P230S (C688T)**			
116			D173G (A518C), F204L (T610C)			
117			**I163T (T488C)**			
118				**L274P (T821C)**		
119	(T-86C)			**D271G (A812G)**		
120				**M275V (A823G)**		
121				F262S (T785C)	E382G (A1145G)	
122		**M1T (T2C)**				
123			T186A (A566G)	Q282L (A845T), V289A (T866C)		
124		G86G (T258C)		**G267S (G799A)**		
125					**N418 frameshift (ΔA1252)**	
126				**I270T (T809C)**		(ΔA + 1612)
127					**N418 frameshift (ΔA1252)**	
128				**T280I (C839T)**		
129		N69S (A206G)	I234V (A700G)			
130	(A-109G, T-42C)					(ΔA + 1612)
131			**R232G (A694G)**			
132		**M1V (A1G)**				
133				E261G (A782G), R321G (A961G)	N423S (A1268G)	
134			**R236G (A706G)**		S328S(A984G)	
135			R200G (A598G)	K309K (A927G)	N510D (A1528G)	(C + 1677 T)
136			**M191T (T572C)**			(A + 1806G)

Each row represents an allele with the protein and DNA substitutions listed by domain. "Δ" indicates a deletion. Alleles with a single amino acid substitution are shown in bold.

linker region may form a salt bridge with a backbone phosphate, which would be abolished by the R236G substitution (Fig. 4b, iii). I163 and P230 are adjacent to one another on the internal surface of beta-sheet strands 1 and 4 (Fig. 4b). Substitutions to Thr or Ser respectively would likely disrupt the fold of the RRM and the conformation of the RNA binding face of the beta-sheet. The I163T substitution is also present, along with additional substitutions in the N- and C-terminal LCDs, in 2 of 3 heat-sensitive alleles of *HRP1* isolated in a previous study (*nab4-4* and *nab4-7*; Minvielle-Sebastia *et al.* 1998).

In RRM2 several of the readthrough substitutions are on the external surface of the RRM, away from the RNA-binding face. An exception is the M275V substitution. M275 is analogous to M191 in RRM1 and appears to make an equivalent 3-bridge cluster with F246, F286, and F288, which interacts with the bases of A2 and U3 (Fig. 4b, iv). Leucine274 buttresses M275 and is substituted with proline in 2 alleles (Table 1 and Fig. 4b, iv). These substitutions are likely to affect RNA binding. K244N in beta-strand 1 could disrupt an internal H-bond with T290 in beta-strand 3 (Fig. 4b). D271G would disrupt a potential interdomain salt bridge with K231 in RRM1 (Fig. 4b, v), which may be important for the correct positioning of the RRMs relative to each other when binding RNA. I270T is adjacent to D271 and could also affect this interdomain interaction. However, G267S and notably T280I are not near the RNA and are surface exposed, indicating that they could cause readthrough by disrupting protein–protein interactions with other termination factors or the RNAP II EC.

Readthrough can be elicited by start codon or frameshift mutations in Hrp1

The only alleles from the recessive readthrough selection that contain substitutions within the ORF but not in either RRM alter Hrp1 expression. We obtained 2 different single-nucleotide substitutions in the AUG start codon: M1T (ACG) and M1V (GUG) (Table 1). In these strains, if translation does not initiate at the Met1 position there are multiple out-of-frame AUG codons before the next in-frame AUG at M126 (Fig. 5a). Furthermore, we deleted amino acids 1-125 and found that this allele is recessive lethal, so translation starting at M126 does not produce functional Hrp1. Since *hrp1-M1T* and *hrp1-M1V* are viable alleles, translation is likely starting at the +1 codon. Both ACG and GUG codons have been shown to be used as start codons in yeast (reviewed in Kearse and Wilusz 2017).

To determine if these alleles express FL Hrp1 protein, we transformed plasmids containing either *HRP1*, *hrp1-M1T*, or *hrp1-M1V* into an *hrp1* disruption strain that contained a *URA3* plasmid with amino-terminally tagged *GFP-HRP1*. The *GFP-HRP1* plasmid was then selected against by plating onto media containing 5-FOA. This allowed us to visually confirm on a Western blot that any FL Hrp1 protein in these strains is from the mutated allele

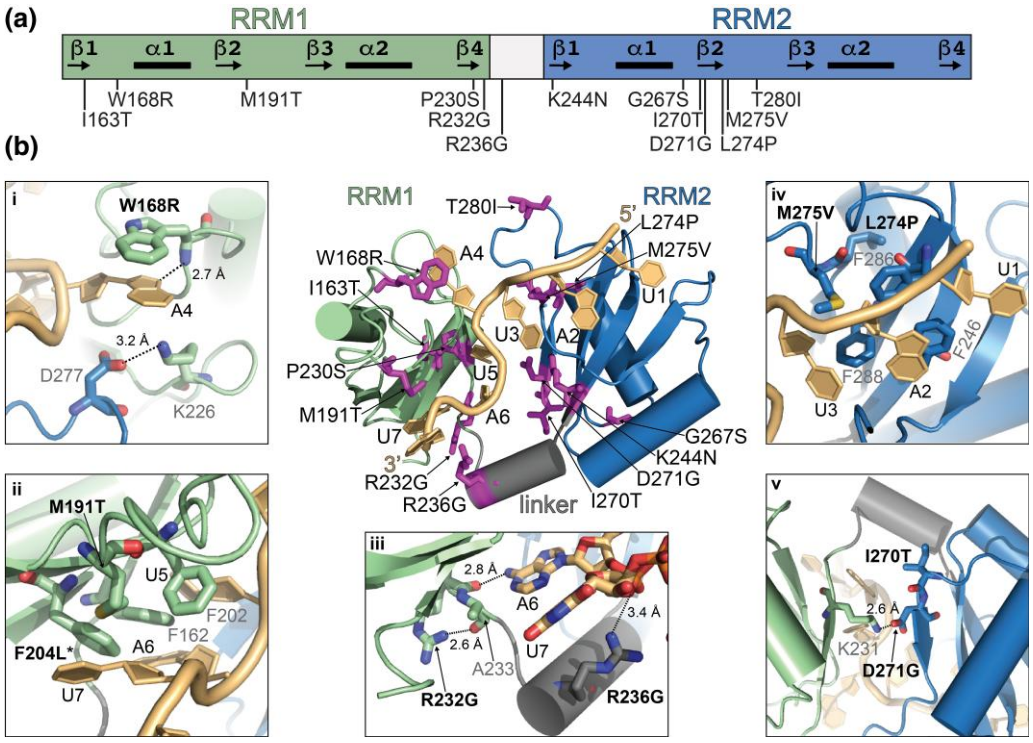

Fig. 4. Viable terminator readthrough substitutions in RRMs 1 and 2 are mostly in the RNA-binding surface. a) Individual substitutions in Hrp1 RRMs 1 and 2 obtained in a selection for viable mutations causing readthrough of the SNR82 terminator. Secondary structure elements are labeled. b) Viable readthrough mutations shown in magenta on structure of Hrp1 RRM1 (green), linker helix (gray), and RRM2 (blue) bound to $(UA)_4$ RNA (gold) (PDB: 2cjk, Pérez-Cañadillas 2006). Panels i–v show interactions that may be disrupted by substitutions from the selection (labeled in bold). Other relevant residues are labeled in gray. Nucleotides are numbered from 5′ to 3′. (*) indicates substitutions from alleles with multiple mutations (see Table 1). i) Stacking interaction between A4 and W168 and a salt bridge between RRM1 and RRM2. ii) Apparent "three-bridge cluster" around M191 involving F162, F202, and F204 that interacts with U5, A6, and U7. iii) Potential hydrogen bonds between A6 and R232 backbone carbonyl, and R236 and RNA backbone. iv) "Three-bridge cluster" in RRM2 around M275 involving F246, F286, and F288 that appears to interact with A2 and U3. v) Substitutions in residues participating in or near the potential salt bridge between K231 (RRM1) and D271 (RRM2).

and not from the *GFP-HRP1* plasmid with an inactivated *URA3* gene (Fig. 5b). As predicted, *hrp1-M1T* and *hrp1-M1V* express FL Hrp1 protein, though at slightly lower levels than wild-type *HRP1*. None of these strains had a band at the expected size for GFP-Hrp1 and there was no evidence of the GFP tag being cleaved off (Fig. 5b, lane 1), indicating that the Hrp1 protein in the M1T and M1V lanes is from the mutated allele. We conducted Western blots on two biological replicates for each strain and found that *hrp1-M1T* and *hrp1- M1V* produce approximately 80 and 60% of the wild-type level of Hrp1 protein, respectively, though the reduction from wild-type was not statistically significant (Fig. 5b and Supplementary Fig. 11b). Initiation of translation at noncanonical start codons typically results in incorporation of methionine as the first amino acid (Kearse and Wilusz 2017). If that is the case for these alleles, the Hrp1 protein made from them has the wild-type sequence. We hypothesize the *hrp1-M1T* and *-M1V* alleles were obtained in the selection because they reduce the cellular concentration of Hrp1, causing readthrough of the SNR82 terminator. However, since the amino-terminus of Hrp1 appears to be an important epitope for the Hrp1 antibody, we cannot exclude the possibility that translation initiation occurring at M126 produces an in-frame, amino-terminally truncated Hrp1 that has a dominant negative effect at the SNR82 terminator but is not detected on our Western blots.

Since translation initiation on the *hrp1-M1T* and *hrp1-M1V* mRNAs is likely much less efficient than with AUG, we predicted that these substitutions compensate for the reduced translation by overexpressing *HRP1* mRNA through increased readthrough of the *HRP1* attenuator. We measured *HRP1* mRNA level by RT-qPCR and found that *hrp1-M1T* causes a 43-fold increase in *HRP1* mRNA, while *hrp1-M1V* causes a 25-fold increase (Fig. 5c). These results suggest that translation initiation is less efficient from the ACG (Thr) codon in this sequence context than GUG (Val) and that neither is very efficient. The *HRP1* attenuator appears to play a significant role in modulating *HRP1* mRNA levels in the cell, though it should be noted that these alleles are plasmid-borne so increased plasmid copy number could account for some of the increase we observed. Also, some of the increased mRNA level could be due to stabilization in the absence of efficient translation.

We also obtained 2 alleles that contain a single-nucleotide deletion in the Asn418 codon that causes a frameshift and premature stop codon 2 amino acids downstream at position 420 (Table 1, Fig. 5a). These alleles are viable even though termination at the premature stop codon at 420 would delete the essential C-terminal region, including the NLS (Fig. 3a). We predicted that these alleles are viable because the ribosome frameshifts back into the correct reading frame at some frequency to produce FL Hrp1 protein. Indeed, Western blots reveal that both of the N418 frameshift alleles overexpress truncated Hrp1 that has an apparent molecular mass consistent with recognition of the premature stop codon (Δ420–534), but both strains also express FL Hrp1 that must derive from frameshifting (Fig. 5b and Supplementary Fig. 11b). This site may be more permissive to frameshifting because the deletion is immediately downstream of a proline-proline dipeptide. Proline codons have been implicated in slowing the

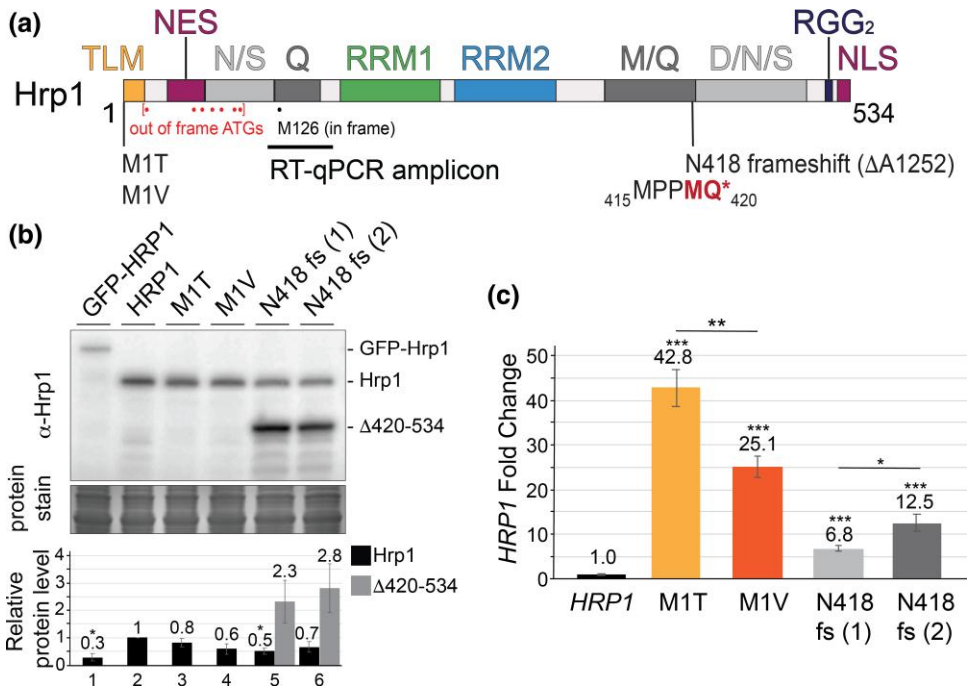

Fig. 5. Potentially lethal mutations in Hrp1 are rescued by autoregulation. a) Start codon substitutions and the N418 frameshift mutation mapped onto Hrp1. Out of frame ATGs before the first in frame ATG downstream of the start codon are indicated with red dots. The predicted effect of the frameshift mutation is shown with red indicating the new reading frame and (*) indicating a premature stop codon. b) Anti-Hrp1 Western blot of cell extracts from haploid strains containing the indicated *HRP1* alleles on low copy plasmids. N418 fs (1) and (2) indicate selection alleles *hrp1-125* and *127*, respectively (see Table 1). Coomassie blue stained gel shown below was used to normalize for total protein loaded. The average, relative protein levels normalized to *HRP1* (lane 2) from 2 biological replicates (see Supplementary Fig. 11b) are shown in black for FL Hrp1 and gray for truncated Hrp1 in the graph below the gel. Error bars represent the SEM and significance between each mutant and wild-type was calculated by a 2-tailed Student's *t*-test indicated with *P*-value < 0.05 (*), <0.01 (**), or <0.001 (***). c) RT-qPCR of total RNA from the indicated haploid strains to produce the *HRP1* amplicon indicated in panel A. Values were normalized to a *CDC19* amplicon. Error bars represent the SEM for 3 biological replicates.

Table 2. Alleles selected for dominant readthrough of the *SNR82* terminator.

Group:	*hrp1* allele:	Substitution:			
		N-term:	RRM1:	RRM2:	C-term:
1	**101**		**G201R (G601A)**, S211S (T633A)		
	106		**F202L (T604C)**		
	107	K54K (A162G)	**L175P (T524C)**		
2	**102**	S155P (T463C)	**G165D (G494A)**	I245I (C735T)	
	103	N53D (A157G, C159T)	**K231R (A692G)**		
	109		**F179S (T536C)**		Q405R (A1214G)
	104 (cs)		G165S (cs) (G493A)		N338S (A1013G)
3	**105**		W168R* (T502C), T219A (A655G)	R317G* (A949G)	
	108	E28G (A83G)	A233T* (G697A)	A272V* (cs) (C815T)	

Each row represents an allele with the substitutions separated by domain. Recessive lethal alleles, as determined by 5-FOA inviability, are shown in bold. Synthetic lethal double mutations are indicated with (*). (cs), cold sensitive (see Supplementary Fig. 12a).

ribosome elongation rate due to inefficient peptidyl transfer (Pavlov *et al.* 2009; Artieri and Fraser 2014) and proline-proline motifs have been shown in *E. coli* to promote ribosome stalling (Tanner *et al.* 2009; Krafczyk *et al.* 2021). This frameshifting must be inefficient given the large amount of truncated protein that accumulates, so we surmised that the N418 fs alleles cause readthrough of the *HRP1* attenuator to increase *HRP1* mRNA expression. RT-qPCR on total RNA from these strains confirmed that expectation. N418 fs (1) shows a 7-fold increase in *HRP1* mRNA while N418 fs (2) shows a 12-fold increase (Fig. 5c). The basis for this modest but statistically significant difference is unknown. Together the Met1 substitutions and N418 frameshift alleles indicate that *HRP1* autoregulation provides resilience to potentially lethal mutations.

The paucity of dominant readthrough mutations in RRM2 suggests a role in protein–protein interactions

The results of the Hrp1 domain deletions and recessive viable mutant selection suggest that RNA binding by both RRMs is important for the recognition of the *SNR82* terminator and that there may be an additional function for RRM2 in complex assembly. We also conducted a selection for dominant readthrough mutations, which requires that the mutated Hrp1 maintains the ability to compete with wild-type Hrp1 at the *SNR82* terminator but is unable to elicit efficient termination. If, for example, a preformed termination complex recognizes the terminator in the nascent transcript, a dominant selection should yield mutations in the

RRM-RNA interface but not in residues required for stable complex formation.

The dominant selection used the same procedure as the recessive selection except the recipient strain contained an intact chromosomal *HRP1* gene and we maintained selection for the *HIS3* marker on the mutated *HRP1* plasmid throughout. *HRP1* plasmids were extracted from the copper-resistant colonies and retransformed into a naïve *cup1Δ* strain containing the *SNR82* reporter plasmid. Plasmids that conferred copper resistance in at least 1 of 2 biological replicates were sequenced to determine the location of the mutation (Table 2). All the dominant alleles had at least one substitution in RRM1 and fit into 3 groups. Group 1 alleles have only a single substitution in RRM1. Group 2 alleles have an additional substitution in the amino- or carboxyl-terminal domain. Group 3 alleles have 3 substitutions, including at least one each in RRM1 and RRM2.

To determine if the dominant alleles are recessive viable, we transformed plasmids containing each allele into an *hrp1* disruption strain bearing a *URA3*-marked *HRP1* plasmid and plated cells onto media containing 5-FOA to select for loss of the wild-type plasmid. We found that all alleles are recessive lethal except for *hrp1*-104, which is cold-sensitive (Table 2 and Supplementary Fig. 12a). For Group 1 alleles, this result indicates that G201R, F202L, and L175P are lethal substitutions. G201 and F202 are on the RNA binding face of RRM1 and the substitutions in these residues would likely disrupt RRM1's interaction with the $(UA)_4$ RNA (Pérez-Cañadillas 2006) (Fig. 6b). F202 is part of the apparent 3-bridge cluster with M191, F162, and F204 (Fig. 6b, ii). L175P would likely disrupt the fold of RRM1.

For the alleles that contain multiple substitutions, we made each substitution individually and determined their recessive viability at 30° and growth at different temperatures (Table 2 and Supplementary Fig. 12a). For the three lethal Group 2 alleles, the lethality was completely attributable to the substitutions in RRM1: G165D, K231R, and F179S. The substitutions in these alleles that are outside of RRM1 supported normal growth at all temperatures tested (Table 2 and Supplementary Fig. 12a). G165 is near the RNA backbone and introduction of an aspartate sidechain at this position would likely cause a steric and charge clash as well as disrupt the potential inter-RRM salt bridge between K226 and D277 (Fig. 6b, i). K231 forms an inter-RRM salt bridge with D271, in which we obtained a substitution to glycine in the recessive readthrough selection (Fig. 6b, iii). Although the K231R substitution would maintain the positive charge, the geometry of the side chain would be significantly altered and the arginine guanidinium group could stack on or between nearby nucleobases, potentially competing with the formation of the salt bridge. The F179S substitution is internal in RRM1 (Fig. 6b) and a less disruptive tyrosine substitution at this position is present in the *nab4-1* allele of *HRP1*, which is heat-sensitive rather than lethal (Minvielle-Sebastia *et al.* 1998).

The remaining Group 2 allele, *hrp1*-104, is viable but cold-sensitive and this phenotype tracks to the RRM1 substitution G165S and not a substitution in the carboxyl-terminal domain, N338S (Supplementary Fig. 12a). We obtained 2 different substitutions in G165, G165S is viable while the more severe G165D is lethal. Thus, all the growth defects of the Group 1 and 2 dominant readthrough mutants can be attributed to substitutions in RRM1.

Interestingly, while both Group 3 alleles are lethal, in each case the 3 constituent amino acid substitutions are viable (Table 2). For allele 105, W168R confers a severe growth phenotype, while T219A and R317G exhibit normal growth (Supplementary Fig. 12a). Thus, lethality is due mostly to W168R but also requires one or both of the other substitutions. W168R is the only substitution that we obtained in both the recessive viable and dominant selections (Supplementary Fig. 13). For allele 108, the A272V substitution in RRM2 confers strong cold-sensitivity, the A233T allele in RRM1 confers weak cold-sensitivity, and E28G exhibits normal growth (Supplementary Fig. 12a). A272 is near several of the recessive selection substitution alleles including D271, which forms an inter-RRM salt bridge with K231 (Fig. 6b, iii and Supplementary Fig. 13). The larger valine side chain at this position might disrupt the salt bridge. The backbone of A233 appears to participate in a salt bridge with R232 that forms an H-bond with A6 and substitution to Thr would likely disrupt this interaction (Fig. 6b, iv).

To determine which of the viable substitutions contribute to readthrough of the *SNR82* terminator, we transformed the ACT1-CUP1 reporter containing this terminator into strains containing each substitution. The mutations S155P, N53D, and Q405R, which are all outside of the RRMs and have no growth phenotypes, did not cause readthrough of the *SNR82* terminator in our copper resistance assay (Fig. 6c and Supplementary Fig. 12b). This result is consistent with the lethal RRM1 substitution in each of these Group 2 strains being responsible for the dominant readthrough phenotype. As predicted by the growth phenotype, G165S phenocopies the readthrough effect of its parent allele, *hrp1*-104, while the other substitution, N338S, elicits no detectable readthrough (Fig. 6c and Supplementary Fig. 12b).

For the Group 3 allele 105, W168R causes a strong readthrough of the SNR82 terminator as well as the slow growth observed on YEPD plates. T219A exhibited no readthrough and R317G caused weak readthrough of the *SNR82* terminator (Fig. 6c and Supplementary Fig. 12b). The location of R317 on the surface of RRM2 far from the RNA-binding region (Fig. 6b) suggests the readthrough phenotype of the R317G substitution could be due to altered interaction with another termination factor or the RNAP II EC. We, therefore, constructed the W168R/R317G double mutant and found that it is recessive lethal, indicating that these 2 substitutions have an additive effect and are responsible for the lethality of the 105 alleles. For *hrp1*-108, we found that A233T in RRM1 caused strong readthrough despite weak cold-sensitivity and A272V in RRM2 causes weak readthrough despite strong cold-sensitivity. The remaining substitution, E28G conferred neither phenotype. We made the A233T/A272V double mutation and found that it was recessive lethal. Thus, for both Group 3 alleles dominant readthrough and lethality are caused by a viable, strong readthrough mutation in RRM1 paired with a weaker readthrough mutation in RRM2. Taken together the dominant selection alleles highlight the importance of RRM1 for NNS terminator recognition. The lack of RNA binding mutations in RRM2 suggests that these mutations do not cause a strong enough readthrough effect with wild-type Hrp1 present or that they prevent mutant *hrp1* from competing with wild-type at the *SNR82* terminator.

Discussion

Hrp1 is an essential RNA binding protein that has been implicated in RNAP II transcription elongation, termination via both the CPA and NNS-dependent pathways and mRNA export. However, the Hrp1 function in these processes is poorly understood. We conducted a structure-function analysis and genetic selections to determine domains and residues important for *HRP1* autoregulation and termination at the Hrp1-dependent snoRNA terminator *SNR82*. We found that most domains of Hrp1 are essential and that the Hrp1 RRMs are not interchangeable. Selections for both recessive viable and dominant readthrough mutations yielded mostly mutations in the RRMs that suggested both RRMs contribute

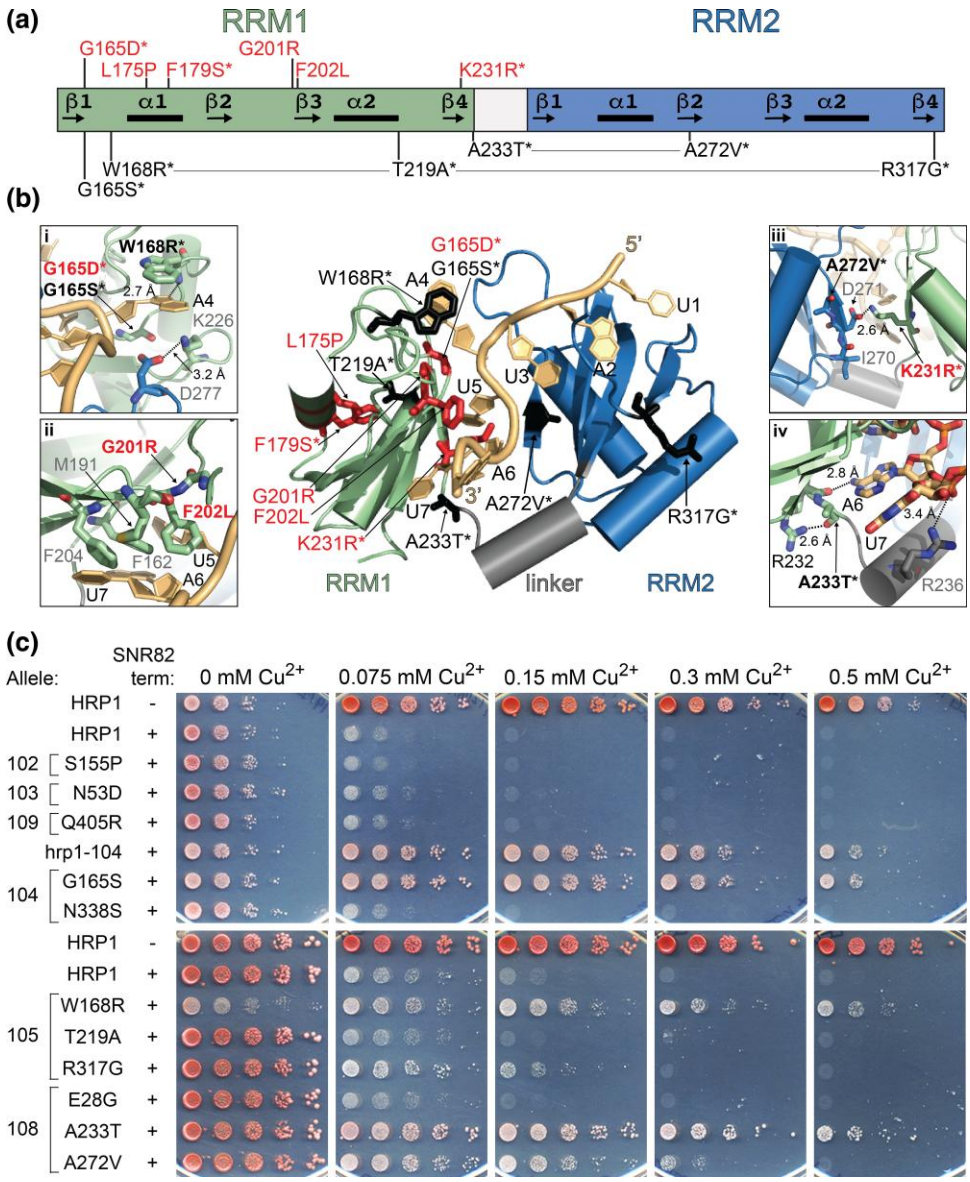

Fig. 6. Dominant readthrough mutations are largely in RRM1. a) Substitutions in the Hrp1 RRMs from the SNR82 dominant readthrough selection. Recessive lethal substitutions are shown in red above and viable substitutions in black below. (*) indicate that allele contained multiple substitutions and lines connect substitutions in the same allele when present in the RRMs (see Table 2). b) Substitutions mapped onto Hrp1 RRM structure with RRM1 (green), linker helix (gray), and RRM2 (blue) bound to $(UA)_4$ RNA (gold) (PDB: 2cjk, Pérez-Cañadillas 2006). Panels i–iv show interactions that may be disrupted by substitutions from the dominant selection shown in black (viable) and red (lethal). Other relevant residues are labeled in gray. Nucleotides are numbered from 5′ to 3′. (*) indicates substitutions from alleles with multiple mutations. i) A4 binding pocket and a salt bridge between RRM1 and RRM2. ii) Apparent "three-bridge cluster" around M191 involving F162, F202, and F204 that interacts with multiple bases in the RNA. iii) Substitutions in residues participating in or near the potential salt bridge between K231 (RRM1) and D271 (RRM2). iv) Recognition of A6 by R232 and A233. c) Serial dilutions of haploid strains containing the indicated alleles of *HRP1* and the SNR82 ACT1-CUP1 reporter were spotted on medium containing the indicated concentration of copper sulfate. Biological replicate shown in Supplementary Fig. 12b.

to RNA binding but RRM2 may also be important for mediating interactions with the RNAP II EC or other termination factors. Recessive viable readthrough substitutions in Met1 and C-terminal frameshift mutations showed that Hrp1 autoregulation provides resilience against potentially lethal defects in Hrp1 expression.

The *hrp1-7* allele may contain separation of function mutations

We found that the previously published NNS attenuator/terminator readthrough phenotype of the *hrp1-7* allele (Kuehner and Brow 2008; Chen *et al.* 2017) is largely due to the M191T substitution in RRM1, but that at least the N345D substitution in the carboxyl-terminal region exacerbates its phenotype. Furthermore, we found that the A195P substitution in *hrp1-7* does not cause readthrough of the *HRP1* attenuator or *SNR82* terminator on its own but appears to result in defective expression of the HRP1-CUP1 reporter gene (Fig. 1b). The A195P substitution could be responsible for the apparent processivity defect of RNAP II in an *hrp1-7* strain (Chen *et al.* 2017). A195 is in a loop in RRM1 and appears to be surface exposed and, therefore, could be involved in the association between Hrp1 and the EC (Supplementary Fig. 3a). While M191 is conserved between Hrp1 and human UA-rich RNA binding Msi1/2 and DAZAP1 A195 is not, suggesting that it may be important for mediating an interaction that is specific to Hrp1 (Supplementary Fig. 2).

Transcriptome analysis of the individual *hrp1-M191T* and *hrp1-A195P* substitutions will be required to determine if the readthrough and positive elongation defects observed in *hrp1-7* are truly separable.

The Hrp1 low-sequence complexity domains contribute to its essential function(s) and NNS termination

Individual deletions of the TLM and NES regions of the Hrp1 N-terminal domain are recessive viable but caused readthrough of both the *HRP1* attenuator and the *SNR82* terminator (Fig. 3d and e). The TLM region is similar to other short linear motifs (SLiMs) including "TIMs", which are present in RNAP II elongation factors and bound by the "TND" domain of TFIIS and other transcription elongation factors (Cermakova *et al.* 2021). Thus, the conserved TLM could be a protein–protein interaction domain that helps localize Hrp1 to the EC. Of the known TND-containing elongation factors, only Dst1/TFIIS, Spn1/Iws1, and Elongin A (Ela1/ELOA1) are conserved in *S. cerevisiae*. Dst1 and Spn1 are both general elongation factors that associate with RNAP II. Dst1 stimulates RNAP II elongation through transcriptional blocks (Noe Gonzalez *et al.* 2021) and Spn1 acts as a histone chaperone (Reim *et al.* 2020), while Ela1 is involved in RNAP II ubiquitination upon encountering DNA damage or other blocks to elongation (Ribar *et al.* 2007). A genome-wide genetic interaction study identified a negative genetic interaction between *hrp1* and *spn1* alleles (Costanzo *et al.* 2016). Further studies are required to determine if the Hrp1 TLM interacts with the TND of any of these proteins.

A putative NES (aa 42–52, see Supplementary Fig. 1) was proposed in a previous study showing that Hrp1 is rapidly exported to the cytoplasm under hyperosmotic stress conditions (Henry *et al.* 2003). This process was shown to be dependent on the nuclear export factor Crm1/Xpo1 and this Hrp1 (LAALQALSSSL) sequence is similar to the binding site for Crm1/Xpo1. Hrp1 has also been shown to interact with Crm1/Xpo1 by yeast-2-hybrid assay (Hammell *et al.* 2002). It is unclear whether this interaction is generally required for Hrp1 export or only under stress conditions as Hrp1 is proposed to exit the nucleus associated with mRNAs (Kessler *et al.* 1997; Kim Guisbert *et al.* 2005). Our finding that the deletion of a region containing this potential NES (*hrp1-ΔNES*) causes readthrough of two NNS terminators could be due to a defect in Hrp1 nuclear shuttling where Hrp1 bound to mRNAs accumulates in the nucleus but is unable to be recycled thus causing a reduced pool of free Hrp1 available to act at NNS terminators. It is also possible that if there is an mRNA export defect, the expression of other NNS factors could be altered causing readthrough of NNS terminators.

The carboxyl-terminal D/N/S LCD is uncharacterized, but we found that it is required for viability. Interestingly, deletion of this region appears to cause a dominant decrease in the level of both mutant and wild-type Hrp1 protein (Fig. 3b). This result suggests the D/N/S LCD normally acts as a negative autoregulatory domain that reduces Hrp1 activity at the *HRP1* attenuator, thus its deletion increases the attenuation of Hrp1 mRNA. A recent study with the tandem RRM-containing splicing factor U2AF2 showed that an intrinsically disordered linker between its RRMs acts as an autoinhibitory domain by competing with RNA for binding to its RRMs to increase binding specificity (Kang *et al.* 2020). Perhaps the Hrp1 D/N/S LCD acts in a similar manner.

HRP1 autoregulation confers resilience to defects in Hrp1 expression

Autoregulation is a common means of controlling the expression and activity of many types of proteins. The level of Hrp1 appears to be tightly regulated, as demonstrated by our finding that doubling the gene dosage of *HRP1* does not cause a significant increase in Hrp1 protein (Fig. 3b). Based on previous studies, this regulation is due at least in part to Hrp1 autoregulation of the transcription of its gene via an NNS attenuator at the 5′ ends of its gene (Kuehner and Brow 2008; Chen *et al.* 2017). Our analysis of Hrp1 protein and mRNA levels in Hrp1 mutant strains showed that strong autoregulation of Hrp1 expression buffered the effects of adverse mutations. The resilience of this feedback regulation was highlighted by the start codon substitutions (M1T and M1V) and N418 frameshift alleles that we obtained in the recessive viable selection for readthrough of the *SNR82* terminator. These strains exhibited increased *HRP1* mRNA levels that mostly compensated for strongly reduced translation efficiency due to the required use of alternative start codons or frameshifting (Fig. 5).

Many hnRNPs contain LCDs that promote aggregation when they are overexpressed. Autoregulation may in part be a mechanism to prevent toxic protein aggregation. While both the Met1 substitution and N418 frameshift strains overexpress *HRP1* mRNA, the N418 frameshift strains produced significantly less *HRP1* mRNA (Fig. 5). We hypothesize that this difference is due to the accumulation of the truncated protein, which is unlikely to enter the nucleus as it is lacking its NLS but still contains the prion-like M/Q-rich LCD. Sustained Hrp1 overexpression has been shown to cause the formation of toxic, cytoplasmic aggregates, mediated by the M/Q LCD, which can sequester wild-type Hrp1 as well as other proteins (Newby *et al.* 2017). The *hrp1-N418fs* strains are likely reaching a steady-state balance between producing enough Hrp1 to support viability, but also preventing too much production of the truncated protein, which may aggregate in the cytoplasm if it accumulates to too high of a level. This balance is similar to what has been observed for TDP-43, another hnRNP protein that forms cytoplasmic aggregates that cause types of amyotrophic lateral sclerosis and frontotemporal dementia (Arai *et al.* 2006; Neumann *et al.* 2006). TDP-43 autoregulates its mRNA levels by regulating alternative splicing of its transcript to maintain the correct level of protein, which along with its controlled nuclear and cytoplasmic shuttling prevent the formation of disease-causing aggregates (Tziortzouda *et al.* 2021). Interestingly, hnRNPD and hnRNPDL both autoregulate and cross-regulate their synthesis by alternative splicing (Kemmerer *et al.* 2018).

The Hrp1 RRMs have distinct functions in NNS termination

Based on the potential antiterminator function for Hrp1, our data are consistent with a model where RRM1 is primarily responsible for scanning the nascent transcript and recognizing termination signals, while RRM2 contributes to RNA binding but is also important for protein–protein interactions with the RNAP II EC and/or other termination factors (Fig. 7). The prevalence of terminator readthrough mutations that are likely to disrupt RRM1 RNA binding and its contacts with more RNA bases than RRM2 when bound to $(UA)_4$ (Pérez-Cañadillas 2006) suggest that RRM1 could provide more selectivity for specific terminator sequences. This model is consistent with previous in vitro studies with a homolog of Hrp1, Musashi 1 (Msi1). Recognition of a core UAG sequence by RRM1 was responsible for most of the RNA binding affinity and specificity, while RRM2 increased the overall affinity (Zearfoss *et al.* 2014). Many of the substitutions in Hrp1 we obtained in the *SNR82* readthrough selections are in residues that are conserved in hnRNPs that bind UA-rich sequences, including Msi1, Msi2, hnRNPD, hnRNPDL, and DAZAP1 (Supplementary Fig. 2). NMR structures of Msi1's individual RRM1 and RRM2 domains bound to their

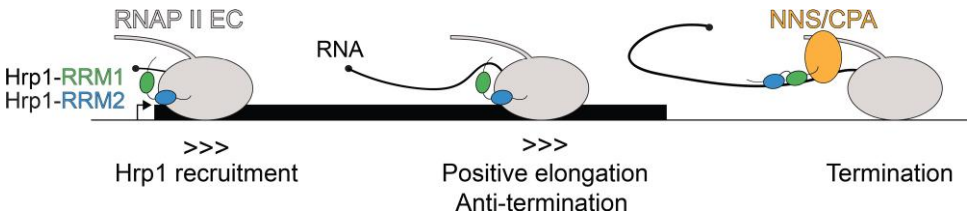

Fig. 7. Model for Hrp1 function in RNAP II transcription. Hrp1 is recruited to the RNAP II EC (gray) near the transcription start site, potentially through interaction with RRM2 (blue). This interaction may promote RNAP II elongation indicated by (>>>) and RRM1 (green) scanning the nascent RNA. Loss of Hrp1 from the EC by recognition of termination signals in the RNA by both RRMs could promote NNS termination. The Hrp1 RRMs could have a similar function in CPA termination at protein-coding genes.

consensus binding sequences, GUAG and UAG, respectively, have been solved and superimpose well onto the Hrp1 RRM1 bound to AUAU and RRM2 bound to AU (Iwaoka *et al.* 2017), which is consistent with similar residues being involved in RNA recognition.

There is no structure of the Hrp1 RRMs in the absence of RNA, but NMR experiments have shown that the relative conformation of the RRMs is flexible without RNA-bound and that the linker helix between the RRMs becomes structured upon binding (Pérez-Cañadillas 2006). These findings suggest that Hrp1 associated with the RNAP II EC could be in a more open, scanning conformation, but that recognition of a high-affinity binding site would induce a conformational change to a more closed, RNA-bound state. This structural transition might result in either the release of Hrp1 from the RNAP II EC, slowing elongation, or transmission of an allosteric signal to the EC that favors termination. Consistent with this hypothesis, we obtained several substitutions in both terminator readthrough selections that are expected to weaken interactions between the RRMs. While G165D is lethal, the G165S substitution is cold-sensitive, indicating that it could stabilize the scanning conformation of Hrp1 and inhibit a conformational change upon RNA binding. G165 is near a potential inter-RRM salt bridge between K226 and D277 that forms part of a binding pocket for A4 with W168 (Fig. 6b, i). The G165S and G165D substitutions could destabilize the RNA-bound state to different extents, causing different levels of readthrough. Similarly, we obtained mutations in both residues that appear to form another inter-RRM salt bridge, K231R, and D271G, as well as in the adjacent residues, I270T, and A272V (Figs. 4b, v and 6b, iii). A272V was the only of these residues tested for temperature-sensitivity, but we found that it is strongly cold-sensitive at 16°C (Supplementary Fig. 12a), which suggests that the bulkier valine sidechain could disrupt the formation of this salt bridge upon RNA binding.

A recent UV-crosslinking study that investigated sites of RNA contact in *S. cerevisiae* nuclear mRNA-binding proteins (Keil *et al.* 2023) identified 4 crosslinked peptides in Hrp1: (1) residues 190–198 of RRM1, which contain M191 and A195, (2) the linker between RRMs 1 and 2, (3) residues immediately C-terminal to RRM2, and (4) residues within the PY-NLS at the C-terminus. These results suggest that domains outside of the RRMs may contribute to RNA binding.

Potential for effects on Hrp1 function at CPA terminators

Although this study focused on two NNS terminators, Hrp1 could also act as an antitermination factor at CPA terminators in protein-coding genes. In CPA site recognition, Hrp1 (CF1B) interacts with CF1A largely through Rna14, which forms a scaffold between Hrp1 and the other RNA binding protein in CF1, Rna15. Rna14 is proposed to bind to the alpha-helical face of the Hrp1 RRMs, opposite the RNA-binding face (Barnwal *et al.* 2012). Interestingly, several of the mutations we obtained in the SNR82 readthrough selection showed large chemical shift perturbations in NMR experiments upon Rna14/Rna15 binding to a preformed Hrp1/RNA complex (Barnwal *et al.* 2012). We obtained substitutions L175P, L274P, I234V (with N69S), V247A (with C301R), and I270T that could disrupt this interface between Hrp1 and Rna14 (Table 1). We expect these mutations may alter Hrp1 recognition of CPA sites at protein-coding genes. Prior studies have also shown that Rna14 can act at NNS terminators including the Hrp1-dependent *DEF1* attenuator (Whalen *et al.* 2018). Whether the effect of these substitutions on recognition of the SNR82 terminator is due to disruption of Hrp1 interaction with Rna14 or some other factor that binds the same region of Hrp1 remains to be determined.

Hrp1 as a general antitermination factor for RNAP II

Hrp1 appears to promote both RNAP II elongation and termination. These potentially opposing functions are consistent with Hrp1 acting as an antitermination factor for RNAP II as initially defined by Logan *et al.* 1987. We propose that Hrp1 bound to the transcription EC promotes RNAP II processivity and that its displacement from the complex in response to terminator elements in the nascent transcript promotes either CPA or NNS termination (Fig. 7). The nature of this potential interaction between Hrp1 and the RNAP II EC is unknown, but a candidate is the Rpb3/Rpb11 dimer on the back of RNAP II. Substitutions in Rpb3 and Rpb11 have been shown to cause dominant readthrough of some NNS terminators (Steinmetz *et al.* 2006b) and are a potential site for Hrp1 to allosterically influence RNAP II elongation. The *S. pombe* homolog of Nrd1, Seb1, binds directly to multiple subunits at the rear of RNAP II via residues in its RNA-binding domain (Kecman *et al.* 2018).

Antitermination factors have been well-characterized in bacterial systems and recently several eukaryotic proteins have been proposed to have this function. The yeast hnRNP protein Npl3 appears to act as an antitermination factor and has been shown to stimulate RNAP II elongation in vitro, prevent premature CPA, and its phosphorylation is proposed to promote its release from the RNAP II EC to allow for recognition of poly(A) sites (Bucheli and Buratowski 2005; Dermody *et al.* 2008). This function of Npl3 is similar to U1 snRNP telescripting, where the U1 snRNP binds to cryptic poly(A) sites in mammalian genes to prevent premature CPA (Kaida *et al.* 2010; Venters *et al.* 2019). The human proteins SCAF4 and SCAF8, which have been proposed to be the human homologs of yeast Nrd1, were also recently shown to prevent the usage of premature poly(A) sites (Gregersen *et al.* 2019). We propose that Hrp1 is also a eukaryotic antitermination factor, though more studies are required to understand the mechanism

by which it regulates the transition between RNAP II elongation and termination.

Data availability

Strains and plasmids are available upon request. The authors affirm that all data necessary for confirming the conclusions of the article are present within the article, figures, tables, and Supplementary material.

Supplemental material available at GENETICS online

Acknowledgments

We thank Michael Henry for the anti-Hrp1 antibody, Pam Silver for the *hrp1-7* allele, Cammie Lesser and Christine Guthrie for the ACT-CUP reporter, Justin Mabin for advice on RT-qPCR, Sam Butcher for insight on methionine-nucleobase interactions, and Jason Kuehner and members of the Brow, Butcher, and Aaron Hoskins labs for discussions.

Funding

This work was supported by NIH grant R35GM118075 to DAB.

Conflicts of interest

The author(s) declare no conflict of interest.

Literature cited

Amodeo ME, Mitchell SPC, Pavan V, Kuehner JN. RNA Polymerase II transcription attenuation at the yeast DNA repair gene *DEF1* is biologically significant and dependent on the Hrp1 RNA-recognition motif. G3 (Bethesda). 2023;13(1):jkac292. doi:10.1093/g3journal/jkac292.

An Y, Wu W, Lv A. A PCR-after-ligation method for cloning of multiple DNA inserts. Anal Biochem. 2010;402(2):203–205. doi:10.1016/j.ab.2010.03.040.

Arai T, Hasegawa M, Akiyama H, Ikeda K, Nonaka T, Mori H, Mann D, Tsuchiya K, Yoshida M, Hashizume Y, *et al.* TDP-43 is a component of ubiquitin-positive tau-negative inclusions in frontotemporal lobar degeneration and amyotrophic lateral sclerosis. Biochem Biophys Res Commun. 2006;351(3):602–611. doi:10.1016/j.bbrc.2006.10.093.

Arigo JT, Carroll KL, Ames JM, Corden JL. Regulation of yeast NRD1 expression by premature transcription termination. Mol Cell. 2006;21(5):641–651. doi:10.1016/j.molcel.2006.02.005.

Arndt KM, Reines D. Termination of transcription of short noncoding RNAs by RNA polymerase II. Annu Rev Biochem. 2015;84(1):381–404. doi:10.1146/annurev-biochem-060614-034457.

Artieri CG, Fraser HB. Accounting for biases in riboprofiling data indicates a major role for proline in stalling translation. Genome Res. 2014;24(12):2011–2021. doi:10.1101/gr.175893.114.

Barnwal RP, Lee SD, Moore C, Varani G. Structural and biochemical analysis of the assembly and function of the yeast pre-mRNA 3′ end processing complex CF I. Proc Natl Acad Sci U S A. 2012;109(52):21342–21347. doi:10.1073/pnas.1214102110.

Boeke JD, Trueheart J, Natsoulis G, Fink GR. 5-Fluoroorotic Acid as a selective agent in yeast molecular genetics. Wu R, Grossman L, editors. Methods in Enzymology, Vol. 154 of Recombinant DNA Part E. San Diego (CA): Academic Press; 1987. p. 164–175.

Bucheli ME, Buratowski S. Npl3 is an antagonist of mRNA 3′ end formation by RNA polymerase II. EMBO J. 2005;24(12):2150–2160. doi:10.1038/sj.emboj.7600687.

Cermakova K, Demeulemeester J, Lux V, Nedomova M, Goldman SR, Smith EA, Srb P, Hexnerova R, Fabry M, Madlikova M, *et al.* A ubiquitous disordered protein interaction module orchestrates transcription elongation. Science. 2021;374(6571):1113–1121. doi:10.1126/science.abe2913.

Chen S, Hyman LE. A specific RNA-protein interaction at yeast polyadenylation efficiency elements. Nucleic Acids Res. 1998;26(21):4965–4974. doi:10.1093/nar/26.21.4965.

Chen X, Poorey K, Carver MN, Müller U, Bekiranov S, Auble DT, Brow DA. Transcriptomes of six mutants in the Sen1 pathway reveal combinatorial control of transcription termination across the *Saccharomyces cerevisiae* genome. PLoS Genet. 2017;13(6):e1006863. doi:10.1371/journal.pgen.1006863.

Connelly S, Manley JL. A functional mRNA polyadenylation signal is required for transcription termination by RNA polymerase II. Genes Dev. 1988;2(4):440–452. doi:10.1101/gad.2.4.440.

Costanzo M, VanderSluis B, Koch EN, Baryshnikova A, Pons C, Tan G, Wang W, Usaj M, Hanchard J, Lee SD, *et al.* A global genetic interaction network maps a wiring diagram of cellular function. Science. 2016;353(6306):1381–1420. doi:10.1126/science.aaf1420.

Dermody JL, Dreyfuss JM, Villén J, Ogundipe B, Gygi SP, Park PJ, Ponticelli AS, Moore CL, Buratowski S, Bucheli ME. Unphosphorylated SR-like protein Npl3 stimulates RNA polymerase II elongation. PLoS One. 2008;3(9):e3273. doi:10.1371/journal.pone.0003273.

Dichtl B, Blank D, Ohnacker M, Friedlein A, Roeder D, Langen H, Keller W. A role for Ssu72 in balancing RNA polymerase II transcription elongation and termination. Mol Cell. 2002;10(5):1139–1150. doi:10.1016/S1097-2765(02)00707-4.

Ganem C, Devaux F, Torchet C, Jacq C, Quevillon-Cheruel S, Labesse G, Facca C, Faye G. Ssu72 is a phosphatase essential for transcription termination of snoRNAs and specific mRNAs in yeast. EMBO J. 2003;22(7):1588–1598. doi:10.1093/emboj/cdg141.

Gibbs CA, Weber DS, Warren JJ. Clustering of aromatic amino acid residues around methionine in proteins. Biomolecules. 2021;12(1):6. doi:10.3390/biom12010006.

Gregersen LH, Mitter R, Ugalde AP, Nojima T, Proudfoot NJ, Agami R, Stewart A, Svejstrup JQ. SCAF4 And SCAF8, mRNA anti-terminator proteins. Cell. 2019;177(7):1797–1813.e18. doi:10.1016/j.cell.2019.04.038.

Hammell CM, Gross S, Zenklusen D, Heath CV, Stutz F, Moore C, Cole CN. Coupling of termination, 3′ processing, and mRNA export. Mol Cell Biol. 2002;22(18):6441–6457. doi:10.1128/MCB.22.18.6441-6457.2002.

Han Z, Libri D, Porrua O. Biochemical characterization of the helicase Sen1 provides new insights into the mechanisms of non-coding transcription termination. Nucleic Acids Res. 2017;45(3):1355–1370. doi:10.1093/nar/gkw1230.

He X, Khan AU, Cheng H, Pappas DL, Hampsey M, Moore CL. Functional interactions between the transcription and mRNA 3′ end processing machineries mediated by Ssu72 and Sub1. Genes Dev. 2003;17(8):1030–1042. doi:10.1101/gad.1075203.

Henry MF, Mandel D, Routson V, Henry PA. The yeast hnRNP-like protein Hrp1/Nab4 accumulates in the cytoplasm after hyperosmotic stress: a novel Fps1-dependent response. Mol Biol Cell. 2003;14(9):3929–3941. doi:10.1091/mbc.e03-01-0854.

Iwaoka R, Nagata T, Tsuda K, Imai T, Okano H, Kobayashi N, Katahira M. Structural insight into the recognition of r(UAG) by Musashi-1 RBD2, and construction of a model of Musashi-1 RBD1-2 bound to

the minimum target RNA. Molecules. 2017;22(7):1207. doi:10.3390/molecules22071207.

Jumper J, Evans R, Pritzel A, Green T, Figurnov M, Ronneberger O, Tunyasuvunakool K, Bates R, Žídek A, Potapenko A, *et al.* Highly accurate protein structure prediction with AlphaFold. Nature. 2021;596(7873):583–589. doi:10.1038/s41586-021-03819-2.

Kaida D, Berg MG, Younis I, Kasim M, Singh LN, Wan L, Dreyfuss G. U1 snRNP protects pre-mRNAs from premature cleavage and polyadenylation. Nature. 2010;468(7324):664–668. doi:10.1038/nature09479.

Kang H-S, Sánchez-Rico C, Ebersberger S, Sutandy FXR, Busch A, Welte T, Stehle R, Hipp C, Schulz L, Buchbender A, *et al.* An autoinhibitory intramolecular interaction proof-reads RNA recognition by the essential splicing factor U2AF2. Proc Natl Acad Sci U S A. 2020;117(13):7140–7149. doi:10.1073/pnas.1913483117.

Kearse MG, Wilusz JE. Non-AUG translation: a new start for protein synthesis in eukaryotes. Genes Dev. 2017;31(17):1717–1731. doi:10.1101/gad.305250.117.

Kecman T, Kus K, Heo D-H, Duckett K, Birot A, Liberatori S, Mohammed S, Geis-Asteggiante L, Robinson C, Vasiljeva L. Elongation/termination factor exchange mediated by PP1 phosphatase orchestrates transcription termination. Cell Rep. 2018;25(1):259–269. doi:10.1016/j.celrep.2018.09.007.

Keil P, Wulf A, Kachariya N, Reuscher S, Hühn K, Silbern I, Altmüller J, Keller M, Stehle R, Zarnack K, *et al.* Npl3 functions in mRNP assembly by recruitment of mRNP components to the transcription site and their transfer onto the mRNA. Nucl Acids Res. 2023;51(2):831–851. doi:10.1093/nar/gkac1206.

Kemmerer K, Fischer S, Weigand JE. Auto- and cross-regulation of the hnRNPs D and DL. RNA. 2018;24(3):324–331. doi:10.1261/rna.063420.117.

Kessler MM, Henry MF, Shen E, Zhao J, Gross S, Silver PA, Moore CL. Hrp1, a sequence-specific RNA-binding protein that shuttles between the nucleus and the cytoplasm, is required for mRNA 3′-end formation in yeast. Genes Dev. 1997;11(19):2545–2556. doi:10.1101/gad.11.19.2545.

Kim Guisbert K, Duncan K, Li H, Guthrie C. Functional specificity of shuttling hnRNPs revealed by genome-wide analysis of their RNA binding profiles. RNA. 2005;11(4):383–393. doi:10.1261/rna.7234205.

Kim M, Vasiljeva L, Rando OJ, Zhelkovsky A, Moore C, Buratowski S. Distinct pathways for snoRNA and mRNA termination. Mol Cell. 2006;24(5):723–734. doi:10.1016/j.molcel.2006.11.011.

Krafczyk R, Qi F, Sieber A, Mehler J, Jung K, Frishman D, Lassak J. Proline codon pair selection determines ribosome pausing strength and translation efficiency in bacteria. Commun Biol. 2021;4(1):589. doi:10.1038/s42003-021-02115-z.

Kuehner JN, Brow DA. Regulation of a eukaryotic gene by GTP-dependent start site selection and transcription attenuation. Mol Cell. 2008;31(2):201–211. doi:10.1016/j.molcel.2008.05.018.

Kuehner JN, Brow DA. Author correction: regulation of a eukaryotic gene by GTP-dependent start site selection and transcription attenuation. Mol Cell. 2019;74(3):634. doi:10.1016/j.molcel.2019.04.013.

Kuehner JN, Pearson EL, Moore C. Unravelling the means to an end: RNA polymerase II transcription termination. Nat Rev Mol Cell Biol. 2011;12(5):283–294. doi:10.1038/nrm3098.

Lange A, Mills RE, Devine SE, Corbett AH. A PY-NLS nuclear targeting signal is required for nuclear localization and function of the *Saccharomyces cerevisiae* mRNA-binding protein Hrp1. J Biol Chem. 2008;283(19):12926–12934. doi:10.1074/jbc.M800898200.

Lesser CF, Guthrie C. Mutational analysis of pre-mRNA splicing in Saccharomyces cerevisiae using a sensitive new reporter gene, CUP1. Genetics. 1993;133(4):851–863. doi:10.1093/genetics/133.4.851.

Licatalosi DD, Geiger G, Minet M, Schroeder S, Cilli K, McNeil JB, Bentley DL. Functional interaction of yeast pre-mRNA 3′ end processing factors with RNA polymerase II. Mol Cell. 2002;9(5):1101–1111. doi:10.1016/S1097-2765(02)00518-X.

Logan J, Falck-Pedersen E, Darnell JE, Shenk T. A poly(A) addition site and a downstream termination region are required for efficient cessation of transcription by RNA polymerase II in the mouse beta maj-globin gene. Proc Natl Acad Sci U S A. 1987;84(23):8306–8310. doi:10.1073/pnas.84.23.8306.

Loya TJ, O'Rourke TW, Reines D. The hnRNP-like Nab3 termination factor can employ heterologous prion-like domains in place of its own essential low complexity domain. PLoS One. 2017;12(10):e0186187. doi:10.1371/journal.pone.0186187.

Luo W, Johnson AW, Bentley DL. The role of Rat1 in coupling mRNA 3′-end processing to transcription termination: implications for a unified allosteric-torpedo model. Genes Dev. 2006;20(8):954–965. doi:10.1101/gad.1409106.

Martin-Tumasz S, Brow DA. *Saccharomyces cerevisiae* Sen1 helicase domain exhibits 5′- to 3′-helicase activity with a preference for translocation on DNA rather than RNA. J Biol Chem. 2015;290(38):22880–22889. doi:10.1074/jbc.M115.674002.

Minvielle-Sebastia L, Beyer K, Krecic AM, Hector RE, Swanson MS, Keller W. Control of cleavage site selection during mRNA 3′ end formation by a yeast hnRNP. EMBO J. 1998;17(24):7454–7468. doi:10.1093/emboj/17.24.7454.

Nedea E, He X, Kim M, Pootoolal J, Zhong G, Canadien V, Hughes T, Buratowski S, Moore CL, Greenblatt J. Organization and function of APT, a subcomplex of the yeast cleavage and polyadenylation factor involved in the formation of mRNA and small nucleolar RNA 3′-ends. J Biol Chem. 2003;278(35):33000–33010. doi:10.1074/jbc.M304454200.

Neumann M, Sampathu DM, Kwong LK, Truax AC, Micsenyi MC, Chou TT, Bruce J, Schuck T, Grossman M, Clark CM, *et al.* Ubiquitinated TDP-43 in frontotemporal lobar degeneration and amyotrophic lateral sclerosis. Science. 2006;314(5796):130–133. doi:10.1126/science.1134108.

Newby GA, Kiriakov S, Hallacli E, Kayatekin C, Tsvetkov P, Mancuso CP, Bonner JM, Hesse WR, Chakrabortee S, Manogaran AL, *et al.* A genetic tool to track protein aggregates and control prion inheritance. Cell. 2017;171(4):966–979.e18. doi:10.1016/j.cell.2017.09.041.

Noe Gonzalez M, Blears D, Svejstrup JQ. Causes and consequences of RNA polymerase II stalling during transcript elongation. Nat Rev Mol Cell Biol. 2021;22(1):3–21. doi:10.1038/s41580-020-00308-8.

Nomura Y, Roston D, Montemayor EJ, Cui Q, Butcher SE. Structural and mechanistic basis for preferential deadenylation of U6 snRNA by Usb1. Nucleic Acids Res. 2018;46(21):11488–11501. doi:10.1093/nar/gky812.

Ozsolak F, Kapranov P, Foissac S, Kim SW, Fishilevich E, Monaghan AP, John B, Milos PM. Comprehensive polyadenylation site maps in yeast and human reveal pervasive alternative polyadenylation. Cell. 2010;143(6):1018–1029. doi:10.1016/j.cell.2010.11.020.

Pavlov MY, Watts RE, Tan Z, Cornish VW, Ehrenberg M, Forster AC. Slow peptide bond formation by proline and other N-alkylamino acids in translation. Proc Natl Acad Sci USA. 2009;106(1):50–54. doi:10.1073/pnas.0809211106.

Pérez-Cañadillas JM. Grabbing the message: structural basis of mRNA 3′UTR recognition by Hrp1. EMBO J. 2006;25(13):3167–3178. doi:10.1038/sj.emboj.7601190.

Porrua O, Libri D. A bacterial-like mechanism for transcription termination by the Sen1p helicase in budding yeast. Nat Struct Mol Biol. 2013;20(7):884–891. doi:10.1038/nsmb.2592.

Proudfoot NJ. How RNA polymerase II terminates transcription in higher eukaryotes. Trends Biochem Sci. 1989;14(3):105–110. doi:10.1016/0968-0004(89)90132-1.

Ray-Soni A, Bellecourt MJ, Landick R. Mechanisms of bacterial transcription termination: all good things must end. Annu Rev Biochem. 2016;85(1):319–347. doi:10.1146/annurev-biochem-060815-014844.

Reim NI, Chuang J, Jain D, Alver BH, Park PJ, Winston F. The conserved elongation factor Spn1 is required for normal transcription, histone modifications, and splicing in *Saccharomyces cerevisiae*. Nucleic Acids Res. 2020;48(18):10241–10258. doi:10.1093/nar/gkaa745.

Ribar B, Prakash L, Prakash S. ELA1 And CUL3 are required along with ELC1 for RNA polymerase II polyubiquitylation and degradation in DNA-damaged yeast cells. Mol Cell Biol. 2007;27(8):3211–3216. doi:10.1128/MCB.00091-07.

Rodríguez-Molina JB, West S, Passmore LA. Knowing when to stop: transcription termination on protein-coding genes by eukaryotic RNAPII. Mol Cell. 2023;83(3):1–12. doi:10.1016/j.molcel.2022.12.021.

Schiestl RH, Gietz RD. High efficiency transformation of intact yeast cells using single stranded nucleic acids as a carrier. Curr Genet. 1989;16(5-6):339–346. doi:10.1007/BF00340712.

Steinmetz EJ, Brow DA. Repression of gene expression by an exogenous sequence element acting in concert with a heterogeneous nuclear ribonucleoprotein-like protein, Nrd1, and the putative helicase Sen1. Mol Cell Biol. 1996;16(12):6993–7003. doi:10.1128/MCB.16.12.6993.

Steinmetz EJ, Brow DA. Ssu72 protein mediates both poly(A)-coupled and poly(A)-independent termination of RNA polymerase II transcription. Mol Cell Biol. 2003;23(18):6339–6349. doi:10.1128/MCB.23.18.6339-6349.2003.

Steinmetz EJ, Conrad NK, Brow DA, Corden JL. RNA-binding protein Nrd1 directs poly(A)-independent 3′-end formation of RNA polymerase II transcripts. Nature. 2001;413(6853):327–331. doi:10.1038/35095090.

Steinmetz EJ, Ng SBH, Cloute JP, Brow DA. cis- and trans-acting determinants of transcription termination by yeast RNA polymerase II. Mol Cell Biol. 2006a;26(7):2688–2696. doi:10.1128/MCB.26.7.2688-2696.2006.

Steinmetz EJ, Warren CL, Kuehner JN, Panbehi B, Ansari AZ, Brow DA. Genome-wide distribution of yeast RNA polymerase II and its control by Sen1 helicase. Mol Cell. 2006b;24(5):735–746. doi:10.1016/j.molcel.2006.10.023.

Tanner DR, Cariello DA, Woolstenhulme CJ, Broadbent MA, Buskirk AR. Genetic identification of nascent peptides that induce ribosome stalling. J Biol Chem. 2009;284(50):34809–34818. doi:10.1074/jbc.M109.039040.

Tuck AC, Tollervey D. A transcriptome-wide atlas of RNP composition reveals diverse classes of mRNAs and lncRNAs. Cell. 2013;154(5):996–1009. doi:10.1016/j.cell.2013.07.047.

Tziortzouda P, Van Den Bosch L, Hirth F. Triad of TDP43 control in neurodegeneration: autoregulation, localization and aggregation. Nat Rev Neurosci. 2021;22(4):197–208. doi:10.1038/s41583-021-00431-1.

Varadi M, Anyango S, Deshpande M, Nair S, Natassia C, Yordanova G, Yuan D, Stroe O, Wood G, Laydon A, *et al*. Alphafold protein structure database: massively expanding the structural coverage of protein-sequence space with high-accuracy models. Nucleic Acids Res. 2022;50(D1):D439–D444. doi:10.1093/nar/gkab1061.

Venters CC, Oh J-M, Di C, So BR, Dreyfuss G. U1 snRNP telescripting: suppression of premature transcription termination in introns as a new layer of gene regulation. Cold Spring Harb Perspect Biol. 2019;11(2):a032235. doi:10.1101/cshperspect.a032235.

Wagner EJ, Tong L, Adelman K. Integrator is a global promoter-proximal termination complex. Mol Cell. 2023;83(3):416–427. doi:10.1016/j.molcel.2022.11.012.

Whalen C, Tuohy C, Tallo T, Kaufman JW, Moore C, Kuehner JN. RNA Polymerase II transcription attenuation at the yeast DNA repair gene, DEF1, involves Sen1-dependent and polyadenylation site-dependent termination. G3 (Bethesda). 2018;8(6):2043–2058. doi:10.1534/g3.118.200072.

Zearfoss NR, Deveau LM, Clingman CC, Schmidt E, Johnson ES, Massi F, Ryder SP. A conserved three-nucleotide core motif defines Musashi RNA binding specificity. J Biol Chem. 2014;289(51):35530–35541. doi:10.1074/jbc.M114.597112.

Editor: E. Tran